

# POLITECNICO OF TURIN

College of Chemical and Materials Engineering

**Master course  
in Materials Engineering**

Master thesis

## **Synthesis and characterization of gold nanoparticles**



**Supervisor (Politecnico of Turin, Italy)**

Prof. Dr. Mario Rosso

**Supervisors (Paul Scherrer Institute, Swiss)**

Prof. Dr. Christian Ludwig

Dr. Andrea Testino

**Advisor (Paul Scherrer Institute, Swiss)**

Dr. Mohammad Andalibi Reza

**Candidate**

Annalise Annoscia

July 2019



To my family and all my friends

*“At the current stage of development,  
it is not an exaggeration to say that the chemical synthesis  
of metal nanocrystals (as well as for other solid materials)  
remains an art rather than a science”.*

(Xia, Y et al. *Angew Chem Int Ed* **48**, 60–103 (2009))



**INDEX**

|   |    |
|---|----|
| Abbreviations.....  | i  |
| List of figures.....  | ii |
| List of tables.....   | v  |
| Acknowledgements.....   | vi |
| Objective of the thesis.....  | 1  |
| 1 Introduction.....   | 3  |
| 1.1 Nanomaterials.....  | 3  |
| 1.2 Classification.....   | 4  |
| 1.3 Characteristics of nanomaterials.....                                   | 6  |
| 1.3.1 Thermal properties.....   | 6  |
| 1.3.2 Optical properties.....   | 7  |
| 1.3.3 Size, shape and functionalization of NPs.....                         | 9  |
| 1.4 Gold nanoparticles (AuNPs).....   | 9  |
| 1.5 Applications.....   | 10 |
| 2 Synthesis of AuNPs in solution.....                                       | 11 |
| 2.1 Chemical synthesis.....   | 11 |
| 2.1.1 Turkevich method.....   | 13 |
| 2.1.2 Colloidal stability.....  | 18 |
| 2.2 Reaction parameters in the Turkevich synthesis.....                     | 20 |
| 3 Nucleation and growth of nanoparticles in solution.....                   | 26 |
| 3.1 Homogeneous and heterogeneous nucleation.....                           | 26 |
| 3.2 Diffusion controlled growth and surface reaction controlled growth..... | 30 |
| 3.3 Mechanisms of nucleation and growth.....                                | 35 |
| 3.3.1 LaMer model.....  | 35 |
| 3.3.2 Finke and Watzky model.....   | 37 |
| 4 Analysis techniques.....  | 40 |
| 4.1 Set up for the synthesis of AuNPs in water solution.....                | 40 |
| 4.2 Measurements in-situ.....   | 42 |
| 4.2.1 Measurement of reduction potential (Eh).....                          | 43 |
| 4.2.2 Measurements of pH and temperature.....                               | 43 |
| 4.2.3 UV-vis spectra evolution.....   | 45 |
| 4.3 Measurements ex-situ.....   | 46 |
| 4.3.1 TEM.....  | 46 |

## INDEX

---

|       |  |    |
|-------|--|----|
| 4.3.2 | UV-vis spectrum .....  | 47 |
| 5     | Experimental section .....   | 49 |
| 5.1   | Materials .....  | 49 |
| 5.2   | Synthesis and method.....  | 49 |
| 5.3   | Preparation phase.....   | 51 |
| 5.4   | Kinetic analysis.....  | 52 |
| 5.5   | Reduction potential and pH measurements in situ .....                    | 52 |
| 5.6   | Temporal evolution of UV-vis spectrum .....                              | 54 |
| 5.7   | Morfological analysis (TEM).....   | 58 |
| 5.8   | Kinetics and thermodynamics of nanoparticles nucleation and growth ..... | 59 |
| 5.9   | Conclusions .....  | 62 |
|       | References .....   | 64 |

## Abbreviations

|                  |  |
|------------------|--|
| <b>NPs</b>       | Nanoparticle   |
| <b>GNP</b>       | Gold Nanoparticle                                      |
| <b>AuNPs</b>     | Gold Nanoparticle                                      |
| <b>CNT</b>       | Classical nucleation theory                            |
| <b>DLVO</b>      | Dejargan, Landau, Verwey, and Overbeek theory          |
| <b>EDL</b>       | Electric Double Layer                                  |
| <b>Cit</b>       | Citrate  |
| <b>SAD</b>       | Sodium acetone dicarboxylate                           |
| <b>DCA</b>       | Dicarboxy acetone                                      |
| <b>SPR</b>       | Surface Plasmon Resonance                              |
| <b>LSPR</b>      | Localized Surface Plasmon Resonance                    |
| <b>TEM/HRTEM</b> | Transmission Electron Microscopy / High-Resolution TEM |
| <b>UV-VIS</b>    | Ultraviolet-Visible Light Spectroscopy                 |
| <b>Abs</b>       | Absorbance   |
| <b>T</b>         | Transmittance  |
| <b>VIS</b>       | Visible light (spectroscopy)                           |
| <b>FWHM</b>      | Full width half maximum                                |
| <b>F-W model</b> | Finke and Watzky model                                 |

## List of figures

|  |    |
|--|----|
| Figure 1.1: Two researchers from IBM in 1989 wrote the initials IBM using 35 xenon atoms on a substrate of nickel employing the STM technology. <sup>3</sup> .....   | 3  |
| Figure 1.2: Splitting of energy levels in quantum dots due to the quantum confinement effect, semiconductor band gap increases with a decrease in the size of the nanocrystal. <sup>4</sup> .....  | 5  |
| Figure 1.3: Melting temperature vs particle size for PbNPs. The effect of miniaturization is responsible for the decrease in $T_m$ of nanostructures. The $T_m$ changes also for the shape of NPs. <sup>7</sup> .....  | 6  |
| Figure 1.4: Schematic representation of surface plasmon (electronic cloud) oscillation under the effect of an electromagnetic field, shows a collective coherent oscillation of the metal conduction electrons with respect to the nanoparticle positive lattice. <sup>8</sup> ..... | 8  |
| Figure 2.1: Several biological sources used in green synthesis of AuNPs. <sup>15</sup> .....   | 13 |
| Figure 2.2: Reactions for nucleation and growth of AuNPs in the Turkevich method. <sup>18</sup> .....  | 15 |
| Figure 2.3: TEM images of the particles synthesized by Chow and Zukoski, (a) 10 min. (b) 30 min. (c) 60 min. (d) 120 min. (e) final particles. <sup>22</sup> .....   | 16 |
| Figure 2.4: The growth mechanism of Turkevich's synthesis described by Polte. <sup>20</sup> ..   | 17 |
| Figure 2.5: Mechanism of nanoparticle growth due to coalescence. <sup>23</sup> .....   | 19 |
| Figure 2.6: Interaction potential between two spherical particles and the dependence from the particle size. <sup>23</sup> .....   | 19 |
| Figure 2.7: The nanoparticle growth based on the concept of colloidal stability. <sup>23</sup> ...   | 19 |
| Figure 2.8: Description of Turkevich method for the synthesis of colloidal gold. <sup>23</sup> ....  | 20 |
| Figure 2.9: Speciation diagram of gold hydroxo-chloro complexes (a) and citrate (b), and final size and polydispersity of AuNPs obtained by standard Turchevich synthesis (c) <sup>25</sup> .....  | 23 |
| Figure 2.10: Mechanism of the Turkevich synthesis <sup>25</sup> .....  | 24 |
| Figure 3.1: Scheme for the classification of the nucleation types .....  | 26 |

Figure 3.2: Diagram of the change of volume free energy,  $\Delta\mu_v$ , surface free energy,  $\Delta\mu_s$ , and of the total free energy,  $\Delta G$ , as a function of nucleus radius, for the nucleation process, explained by the existence of a critical nucleus radius. All the particles under this critical size dissolve in the solution; above the critical size, the particles have enough energy (they are thermodynamically stable) for the nucleation.<sup>30</sup> ..... 27

Figure 3.3: Effect of the temperature on the dimensions of thermodynamically stable spherical particles, with  $T_E > T_1 > T_2 > T_3$ , where  $T_E$  is the equilibrium temperature.<sup>30</sup> . 28

Figure 3.4: Contact angle of the nucleus with an active center during the heterogeneous nucleation.<sup>31</sup> ..... 29

Figure 3.5: Microscopic (left) and macroscopic (right) views of the diffusion layer structure, where  $M_b$  is the concentration of solute in the bulk solution  $M_s$  is the concentration of the solute at the solid/liquid interface, and  $M_r$  is the solubility of the spherical particle of radius  $r$ .<sup>32, 33</sup> ..... 30

Figure 3.6: The solute concentration profiles of diffusion-controlled and reaction-controlled growth modes.<sup>33</sup> ..... 32

Figure 3.7:  $1KDrdrdt$  vs  $r$  for diffusion controlled growth with an infinite diffusion layer.<sup>31</sup> ..... 34

Figure 3.8: The LaMer model of nucleation and growth nanoparticles.<sup>34</sup> ..... 35

Figure 4.1: Setup for synthesis and characterization in situ of colloidal gold..... 41

Figure 4.2: a) Glass jacketed vessel reactor with three electrodes for measurement of Eh, pH&T, UV-vis spectrum upon the magnetic stirrer. b) Pipetman L P500L, 500-5000 $\mu$ L for the hot injection ..... 41

Figure 4.3: Thermo Fisher Scientific bath Haake S7 ..... 42

Figure 4.4: Metrohm combined gold ring electrode with a ceramic pin diaphragm... 43

Figure 4.5: Metrohm combined pH electrode with integrated Pt1000 temperature sensor and fixed cable ..... 43

Figure 4.6: Front 907 Titrando.<sup>40</sup> ..... 44

Figure 4.7: Set up for recording the evolution of the UV-vis spectra of colloidal gold during the synthesis: a DH-mini-2-GS UV-vis-NIR light source<sup>41</sup>, a miniature flame spectrometer USB2000+XR1<sup>42</sup>, an ocean optics bifurcated fiber optic, and an ocean optics transmission dip probe T300 serie immersed in the solution contained in the glass vessel..... 45

|  |    |
|--|----|
| Figure 4.8: TP300 Transmission dip probe by ocean optics for UV-vis-NIR with 1 cm optical path length. ....  | 46 |
| Figure 4.9: Varian Cary 4000 UV-vis-NIR Spectrophotometer. <sup>45</sup> .....   | 47 |
| Figure 4.10: A simple representation of how a spectrophotometer functions. <sup>46</sup> .....   | 48 |
| Figure 5.1: Measurements of Eh and pH of the solutions in situ .....   | 52 |
| Figure 5.2: Scheme of two reaction pathway for the formation of gold nanoparticles by citrate reduction. <sup>48</sup> .....   | 54 |
| Figure 5.3: Temporal evolution of UV-vis spectrum during the syntheses of colloidal gold solutions .....   | 55 |
| Figure 5.4: Illustration for a qualitative analysis of the synthesis of quasi-spherical gold nanoparticles though temporal evolution UV-vis spectrum.....                    | 55 |
| Figure 5.5: FWHM vs time. $FWHM = (\lambda_i - \lambda_{max}) * 2$ . where $\lambda_i$ is the point of the $Abs_{max}/2$ to the red of $\lambda_{max}$ . <sup>49</sup> ..... | 56 |
| Figure 5.6: TEM micrographs ad histograms of gold nanoparticles. ....  | 58 |
| Figure 5.8: The kinetic curves of AuNPs formation .....  | 60 |
| Figure 5.9: Plots of $\ln k$ vs $1/T$ to determine the activation energies in conditions of higher pH (on left) and of lower pH (on right). ....                             | 61 |

## List of tables

|   |    |
|---|----|
| Table 2.1: Reactivity of auric precursor ions pH dependent .....                          | 14 |
| Table 5.1: Synthesis conditions at the beginning of the reaction for each solution. .     | 50 |
| Table 5.2: Some significative values of pH during the reactions .....                     | 53 |
| Table 5.3: Characteristics of UV-vis spectrum, morphological parameters of AuNPs<br>..... | 59 |

## Acknowledgements

This work was developed in the Paul Scherrer Institute from Villigen in Switzerland, thanks to Prof. Dr. Christian Ludwig, head of the Chemical Processes and Materials Group, and to the Dr. Andrea Testino, who gave me the possibility to stay at the Institute, alongside highly qualified people, for six months.

I take the opportunity to thank every member of Prof. Ludwig's research group:

Mohammad Reza Andalibi, Carino Agnese, Debora Foppiano, Maxim Florentina Violeta, Patil Ajay Bhagwan, Bavish Patel, Mohamed Tarik, Tobias Borgmeyer, Rudolf P.W.J. Struis, Albert Schuler and Sonia Barzgar. It was a great honor for me to know each of them for their warm welcome and high professionalism.

My sincere thanks go to Dr. Mohammad Reza Andalibi, a really capable young engineer to whom I owe the success of this thesis work.

I could not have imagined a better guide for the development and writing of this Master thesis. I was lucky enough to know a singular person for patience, availability and great knowledge, an advisor and a mentor who taught me a lot, both professionally and humanly.

I would like to express my gratitude to my supervisor Prof. Dr. Mario Rosso of Politecnico of Turin, in Italy, who promptly supported me in this unique experience. His kindness and positivity make him a man with a noble soul, as well as being a professional recognized inside and outside the academic environment, but above all among students.

Another professor who I want to mention and thank for his availability and professionalism is Prof. Michele Resta of "Liceo Scientifico Linguistico G.C. Vanini" of Casarano, in Lecce (Italy), a person I will never stop learning from.

To all my cousins and friends who live in Switzerland and were warm with me.

Vito Rizzello and his wife Lucia, Saverio De Marco and his wife Melania, Letizia Rizzello and her partner Stefano, Michele Musto and his wife Maribelle, David and his wife Lucia, Salvatore Cera and his partner Simone, Yusuf and his wife Tiziana,

aunt Maria Vita Annoscia, Anna Solombrino, Ada Difonzo, Michele Difonzo and Davide Difonzo.

My immense gratitude goes above all to my cousins Lucia Cera and her husband Vito Rizzello, who welcomed me into their home, helping and supporting me in this experience of studying abroad. For me, they are my second family in Zürich.

I want to say thanks also to my colleagues and friends of the Politecnico of Turin: Francesca Benevnto and her boyfriend Antonio, Roberto Nasi, Francesca Tagliafierro, Carola Sabatini and, in particular Mariatilde Leo. I am grateful to have met such good people to whom I wish all the best possible.

Another huge recognition goes to my second family in Turin: the two retired nurses of the Le Molinette hospital, Ms Maria Briatore and Ms Maria Merli, for me, two sisters, two mothers, two grandmothers, two angels from Heaven.

To all my relatives and friends who live in Milano, Lecce, Ruffano and Taurisano I would like to thank them for existing in my life: my aunt Assunta Attanasio, my cousins Lorena De Vitis, Antonella D'Amico, all my friends Ginetta Gravante, Alberto Constantini, Rocco Stradiotti, Giorgia De Benedictis and Mirella Preite.

Last but not the least, I would like to thank my sister Gisella Annoscia and my brother Rocco Annoscia, my two heroes; and my parents Attanasio Cristina and Annoscia Francesco, the rocks and the pillars of my life.

My heart goes to my family that pours me the unconditional love every day, without any merit of mine.



## Objective of the thesis

This work of thesis focuses on the synthesis of Gold nanoparticles via wet chemical reduction, according to the method described by Turkevich in his publication of 1951, probably the most common procedure for the synthesis of gold nanoparticles in aqueous suspension.

The keen interest in this well-known synthesis is due to the fact that it allows the quasi-spherical and the monodisperse gold nanoparticles formation with high stability and reproducibility

Although many efforts have been made to synthesize gold nanoparticles of different sizes and shapes, only a few publications describe the mechanisms of nucleation and growth, and how, for example, synthesis parameters influence the morphology of gold nanoparticles (GNPs or AuNPs).

The purpose of this thesis is the synthesis of colloidal gold by monitoring pH, temperature, reduction potential and UV-vis spectra in situ, to understand the temporal evolution of GNPs in terms of nucleation and growth.

The kinetic data are compared with the analysis ex-situ, such as TEM images and UV-vis spectra at room temperature, to describe the morphology and the distribution of nanoparticles and their stability.

Through the study of the synthesis reactions, an explanation of the nanoparticle growth will be provided, comparing the classical and more recently developed mechanisms.

In addition to a qualitative analysis of the gold nanoparticle formation mechanism, we will attempt to provide quantitative data on the kinetics and thermodynamics of the synthesis process, using the simplest models known in the literature.

In particular, from the study of the experimental data, we will try to understand the mechanism of growth of the quasi-spherical nanoparticles, and to evaluate the applicability of the Finke Waztkey kinetic model to extract the nucleation and growth rate constants, and to find the activation energy of the two processes, through the Arrhenius law. In conclusion, we will provide one study of these systems with the

## OBJECTIVE OF THE THESIS

---

description of the growth process from a different perspective with respect to the classical model.

The structure of this thesis is the following. The first chapter is an introduction about the nano world and how the properties of the matter change in the nanoscale.

It will be provided also a brief description of the gold nanoparticles and their applications.

The second chapter is dedicated to the synthesis of gold quasi-spherical nanoparticles in solution, with particular attention to the Turkevich method, the colloidal stability and all the parameters that influence the synthesis.

The third chapter is about the description of nucleation and growth mechanisms, and here, it will be described the LaMer model and the Finke Watzky model for the nucleation and growth of the gold nanoparticles.

The last two chapters deal the work made in the laboratory: in the fourth chapter, there is the description of the analysis techniques used to characterize gold nanoparticles; while the fifth chapter is reserved for the experimental section with the presentation and interpretation of the data, and finally the conclusions of this work are present.

# 1 Introduction

## 1.1 Nanomaterials

Recently, scientific research is focusing its attention on the world of nanomaterials, whose characteristic is that of having one or more dimensions in the range of 1-100 nm (1 nm corresponds to  $10^{-9}$  m).

Nowadays, this class of materials is employed in many fields of our life, for example in the field of electronics, catalysis, optics, biology, and medicine. Nanoscience is the study of these materials, while nanotechnologies are their applications.

Although the concepts of nanoscience and nanotechnologies seem to be new, in reality, nanomaterials were present since ancient times in the glass and ceramic industries, and even in the vegetable and animal world it is possible to identify the presence of nanomaterials.<sup>1</sup>

The Nobel Prize Richard Feynman advanced times by claiming as follows: "The principles of physics, as far as I can see, do not speak against the possibility of maneuvering things atom by atom". He had also stated that, in the future, we would be able to "write the entire 24 volumes of the Encyclopedia Britannica on the head of a pin" (Feynman 1960).<sup>2</sup>

Some years later with the inventions of the Scanning Tunneling Microscope STM (1981) and the Atomic Force Microscope AFM (1986), it was possible to investigate and manipulate the nanomaterials atom by atom as predicted by Richard Feynman.

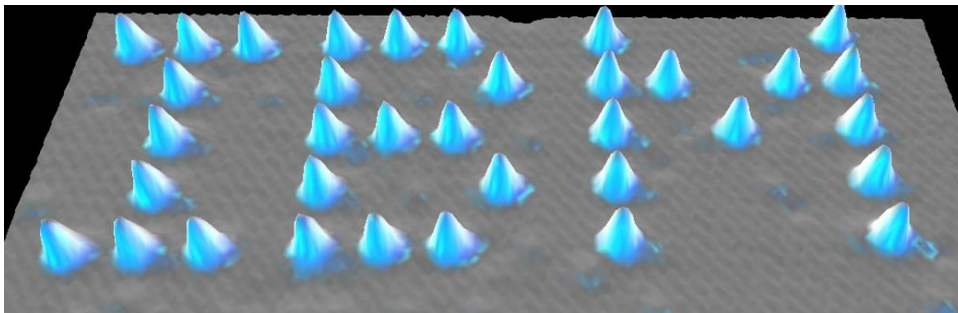


Figure 1.1: Two researchers from IBM in 1989 wrote the initials IBM using 35 xenon atoms on a substrate of nickel employing the STM technology.<sup>3</sup>

### 1.2 Classification

Nanomaterials exhibit a larger surface area and this makes them more chemically reactive, and the resulting quantum effects can change the physics that explains the matter at the nanoscale, influencing their properties.

Materials produced in nanoscale in one dimension, or in two dimensions or in all three dimensions, are classified as:

**0D** (nanoparticles)

**1D** (nanotubes, nanofibers etc.)

**2D** (nanofilms or nanolayer)

**3D** (massive nanomaterials: nanocomposites, mesoporous, and nanostructured)

The properties of nanomaterials are so different from their larger form because they are particularly influenced by surface atoms, which are more numerous than bulk ones.

When a material is close to the nanometer, the chemical-physical properties are completely new and influenced by the particle size. Metals, for examples, become fluorescent and emit light of a different color depending on the size of the particles. Already in the windows of some Gothic churches (e.g. Nôtre Dame), the colors are given not by different elements but by a different dimension of the same elements.

There are two methods to build nanomaterials, by 'top-down' techniques, producing nanostructures starting from macro materials, and by 'bottom-up' techniques, where the nanomaterials are produced atom by atom or molecule by molecule. This is possible through self-assembly or using tools to move each atom or molecule individually, but this second route does not find an industrial application.

Examples of nanostructured objects are tennis rackets, baseball bats, water filters, textiles, creams, cosmetics, disinfectants, etc. In nature, an example is the gecko's fingertips, covered by billions of nanometric bristles able to establish interactions of Van der Waals type with the surface atoms.

The nanometric scale represents a boulder zone, where it realizes the passage between the macroscopic world, regulated by the laws of classical physics, and the atomic scale, dominated by quantum mechanics.

Some metals and metalloids can self-aggregate and give rise to extensive regular size nanostructures, which possess special intermediate properties between those of

an atom, or a single one molecule, and those of a solid. These nanoaggregates, called nanoclusters, can exhibit a significant separation between contiguous energy levels, and these differences between the energy levels can generate transitions in the region of the visible spectrum, and the longer the wavelength of the emitted color, the larger the diameter of the quantum grains.

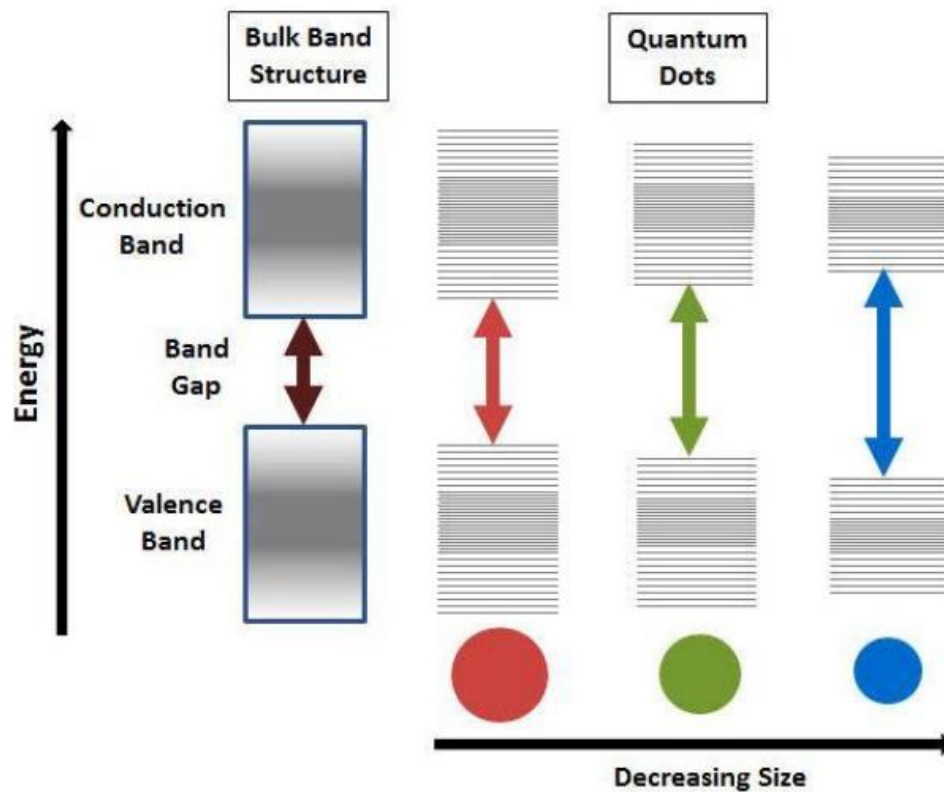


Figure 1.2: Splitting of energy levels in quantum dots due to the quantum confinement effect, semiconductor band gap increases with a decrease in the size of the nanocrystal.<sup>4</sup>

The energy gap between the valence and conduction bands affects various properties, such as intrinsic conductivity, optical transitions, or electronic transitions. Therefore, any variation of the gap alters the physics and chemistry of the material. When the particles are reduced to the dimensions of the nanometer scale, the band gap is very different from that of the bulk, and the same material can exhibit various colors according to its size, and in particular, the band gap increases, as the size decreases (fig.1.2).<sup>5</sup>

## 1.3 Characteristics of nanomaterials

### 1.3.1 Thermal properties

Nanomaterials can have different morphologies according to the different aspect ratio that is the ratio between the maximum and the minimum size. Of course, the spherical nanoparticles have an aspect ratio almost equal to 1 and they are thermodynamically more stable with respect to other nanomaterials of different morphology because they have the least surface energy. Spherical particles of 1-100 nm are called usually nanoparticles, while the term nanocluster or cluster indicates nanoparticles of about 4 nm in diameter.<sup>6</sup>

The shape and size are the most important parameters that affect the performance of the nanoparticles, and their control allows to confer the desired physical, chemical, and mechanical properties. An explanatory example of this aspect is the melting temperature depression of nanoparticles as a function of their size and shape (fig. 1.3).

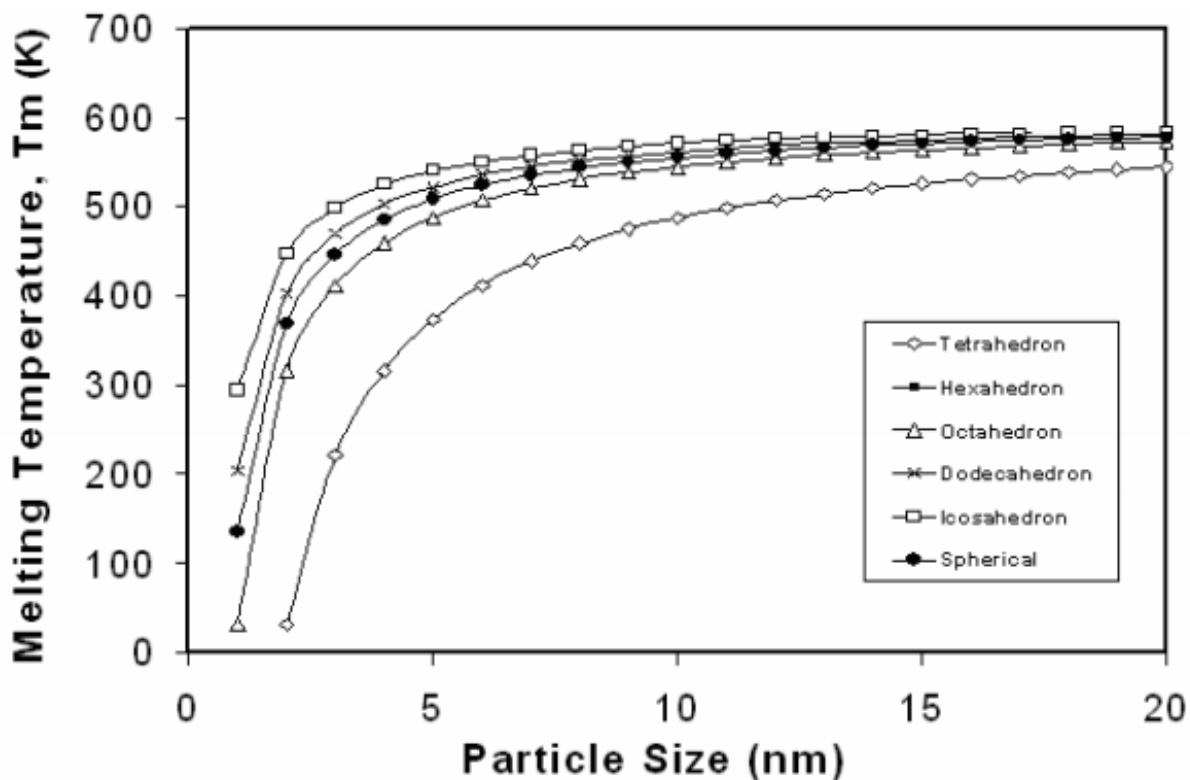


Figure 1.3: Melting temperature vs particle size for PbNPs. The effect of miniaturization is responsible for the decrease in  $T_m$  of nanostructures. The  $T_m$  changes also for the shape of NPs.<sup>7</sup>

It has been experimentally observed that, when the particle size approaches the sub-20 nm range, the surface area is larger than bulk materials, drastically altering their thermodynamic properties, the melting temperature decreases, and in particular, it depends on the ratio of surface atoms and the total atoms.

Experimentally there are two evident aspects: the melting temperature is similar for the larger nanoparticles regardless of shape, but it differs significantly for smaller nanoparticles, and even their shape affects the melting temperature, in fact, different melting temperatures are expected for smaller nanoparticles with the same size but of different shape.

A general equation for the size and shape dependent melting temperature of nanocrystals can be expressed as:

$$T_{mnp} = T_{mb} (1 - N/2n)$$

Here,  $n$  is the total number of atoms of nanoparticles,  $N$  is the number of surface atoms, while  $T_{mnp}$  and  $T_{mb}$  are the melting temperatures of the nanoparticles, and their bulk material respectively.<sup>7</sup>

### 1.3.2 Optical properties

The ability to fabricate nanoscale-sized structures has led to the discovery of useful properties, such as their optical response. Nanomaterials exhibit interesting optical properties that depend on their size, shape, and distribution. If the particles are of nanoscale in size, the reflection of the light is more complex, due to their very high surface area, and their color is a combination of the reflected, absorbed and scattered waves. In particular, metal nanoparticles strongly scatter light and their extinction spectra are a combination of the absorption and scattering. These interactions are strongly influenced by the size, shape and the medium in which the particles are dispersed.

The unique optical properties of noble metal nanoparticles are evident like strong extinction bands in the visible spectrum that are not present in the spectrum of the bulk metal. The extinction spectra of metal nanoparticles can be treated in terms of classical electromagnetism, and Mie proposed the first model, still used today (Mie, 1980). When the oscillating electromagnetic field of the light interacts with metal nanoparticles, causing a collective coherent oscillation of the conduction electrons, a

## CHAPTER 1: INTRODUCTION

---

plasmonic oscillation known as localized surface plasmon resonance (LSPR) takes place, because, at a particular frequency of the light, this process is resonant, and is responsible for the strong extinction band exhibited by the nanoparticles. The resonance occurs when the real part of the metal's dielectric function and the dielectric function of the surrounding medium are the same.

When the resonance frequency (LSPR) falls within the visible spectrum, the particles exhibit vibrant colors that depend on the resonance.

In the other hand, the color of the nanoparticles can be precisely regulated controlling the particle size, the shape or the surrounding medium.

It is well known that LSPR can be advantageous for a number of engineering applications, such as light-emitting diodes (LEDs), sensors, solar cell, electronics, and for medical imaging, for two main reasons: LSPR is tunable changing the composition of nanoparticles, their size and shape; and moreover, LSPR is sensitive to the local environment.

Metal nanoparticles such as silver and gold have the LSPR in the visible range, then they are easy to prepare in different sizes and shapes and they have a surface compatible with a variety of ligands. Therefore, these nanoparticles have gained popularity among the researchers, in particular, for the development of optical sensors and imaging labels.<sup>8</sup>

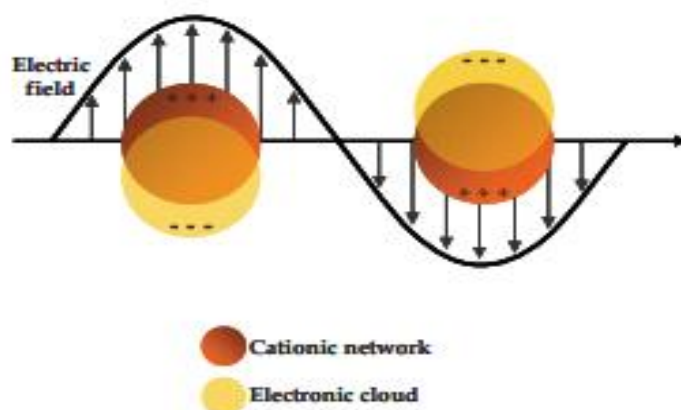


Figure 1.4: Schematic representation of surface plasmon (electronic cloud) oscillation under the effect of an electromagnetic field, shows a collective coherent oscillation of the metal conduction electrons with respect to the nanoparticle positive lattice.<sup>8</sup>

### **1.3.3 Size, shape and functionalization of NPs**

All the properties of metal nanoparticles depend on their size and shape, so much attention has been given to their control. Because of their very small size, nanoparticles are used in biomedicine for the drug delivery, for diagnostic and in chemotherapy, since they respond to a magnetic field and transfer the thermal energy to the tumor cells, working as hyperthermic agents. Nanoparticles, being extremely small, have also a high surface area, hence their surface can be easily modified for many applications in biological sciences.

Futhermore, the interaction of nanoparticles with blood vessels is fundamental in the prevention of cardiovascular diseases.<sup>9</sup>

### **1.4 Gold nanoparticles (AuNPs)**

Gold nanoparticles have physical properties very different from bulk gold that is yellow and inert, while colloidal gold nanoparticles exhibit a wine red color and are anti-oxidant. The colloidal gold is a suspension of sub-micron nanoparticles in a solvent, usually water. Depending on their interactions and self-assembly, their properties change. Gold nanoparticles come in different sizes and shapes. In the past, colloidal gold nanoparticles were used by artists since they have vibrant colors according to their size and shape and interaction with the visible light. More recently, their unique optoelectronic properties are employed in different fields since their optical properties are tunable by changing size, shape, surface, and aggregation state. Futhermore, gold nanoparticles are non-cytotoxic and have a large surface area, so they are available for modification with molecules and specific biomarkers. In particular, they can easily travel into the target cells and release a high drug content. Hence, gold nanoparticles are employed in biomedical science as therapeutic agents or vaccine carriers, with particular emphasis on cancer treatment.<sup>9</sup>

### 1.5 Applications

AuNPs are very versatile and offer a variety of applications in electronics, medicine, food industry, catalysis and cosmetics.

In recent years, the research has highlighted as the properties of selectivity, stability, functionality, and minimized side effects of AuNPs can be employed in medicine.

AuNPs can be used for the releasing of therapeutic molecules, through the absorption of the NIR light, to eradicate cancer cell. For their unique properties, they can work as drug carriers, moreover, their SPR is tunable, making AuNPs some extraordinary molecular nanoprobe for the detection and monitoring of the target molecules. In particular, the use of AuNPs as drug delivery systems has proven to be more effective for the treatment of malignant brain tumors than conventional therapies.<sup>9</sup>

In addition to be used as drug carriers and radiation sensitizers, gold nanoparticles are employed also as the light-heat converters for cancer treatment. In hyperthermia therapy, the particles contained in tumor cells can rapidly convert the absorbed Near-IR light into heat, killing the tumor cell, and leaving healthy ones intact.

The affinity with various biomolecules opens the doors for the diagnostic and treatment not only of cancer, but also of HIV, heart diseases, and genetic diseases.<sup>10</sup>

In the field of sensors, AuNPs can reveal if a food is good to consume or not, and also the presence of pollutants in the environment. In fact, sensors based on gold nanoparticles are used in general for the detection of protein, pollutants and other molecules, also playing an important role in protecting the environment. AuNPs, in particular, prove to be excellent adsorbents for the removal of levels of mercury from drinking water and recently there is a strong use of nanoparticles of noble metals for water purification and contaminant detection.<sup>11</sup>

Several studies on the gold nanoparticles have also led to building catalytic systems for the oxidation of CO into CO<sub>2</sub> at very low temperature. The high catalytic activity of AuNPs has allowed the development of catalysts gold based for fuel cell applications.<sup>12</sup>

## 2 Synthesis of AuNPs in solution

### 2.1 Chemical synthesis

It was 1850 when Faraday opened the doors to the synthesis of colloidal gold solutions by reducing gold chloride with phosphorous, since then many efforts have been made to synthesize AuNPs, controlling their size, shape and surface functionality, for their fascinating properties and promising applications.<sup>13</sup>

In 1951 Turchevich and al. proposed the reduction of tetrachloroauric acid ( $\text{HAuCl}_4$ ) with trisodium citrate ( $\text{Na}_3\text{Ct}$ ) in boiling water ( $100\text{ }^\circ\text{C}$ ), where the citrate acts as both reducing and stabilizing agent. G. Frens, in 1973, described the same procedure changing ratio between the gold precursor salt and the citrate, to obtain control of the size of AuNPs in the range of 16–147 nm.<sup>14</sup>

The “Turkevich method” allows the synthesis of colloidal gold nanoparticles of diameter 10-20 nm, with high stability. Even today, this method is used and modified for its level of simplicity and reproducibility, even though so far, the research has not lead to an understanding of the growth process, since the theories are multiple and inconsistent.

However, in literature, it is possible to find some studies about the role of pH, temperature and sodium citrate concentration, to elaborate a growth model of AuNPs.

In 1994 Brust presented a two-phase process to synthesize 1.5 nm -5.2 nm gold nanoparticles, by using thiol ligands as a capping agent and reducing agent, and sodium borohydride ( $\text{NaBH}_4$ ) as a second reducing agent. In this method, there are two phases, a water phase and an oil phase, and then a phase transfer agent such as tetraoctylammonium bromide (TOAB) that transfers the gold salt from aqueous solution to the oil solution (toluene). With this method, it is possible to control the particle size through the ratio of  $\text{HAuCl}_4$  and  $\text{NaBH}_4$ , and the reaction temperature.<sup>15</sup>

In 2003 David J. Schrifin described a simple purification protocol of AuNPs from the TOAB impurities that can dramatically affect their properties.<sup>16</sup>

## CHAPTER 2: SYNTHESIS OF AuNPs IN SOLUTION

---

Turkevich and Brust-Schiffrin methods allow to obtain monodisperse spherical AuNPs, while the most suitable technique for having the other nanostructures of AuNPs, is surely, the seeded growth method. In this case, a strong reducing agent is employed to form the seeds of nanoparticles that are used in a solution containing metal salt, a weak reducing agent and a structure-directing agent.

By modifying their concentrations, it is possible to control the geometry of the nanoparticles.

Another easy way to synthesize AuNPs is, without doubt, the digestive ripening, where a hot colloidal suspension is in contact with alkanethiols, and in this process, different ligands are used to obtain a product highly monodisperse. In the digestive ripening, the greater particles dissolve, while those smaller grow, in contrast of what happens during the Ostwald ripening.

More recently, alongside these methods, the scientific community has found new synthesis strategies without toxic byproducts, the so-called green methods.

In fact, several publications show, how it is possible the reduction and the capping of AuNPs by using plants or plants extract with the gold salt. Of course, size and shape are tunable by changing the pH, temperature, and concentrations of reagents.

In the green methods, also several bacteria, yeasts, and biomolecules are used to synthesize AuNPs of different size (fig.2.1).<sup>15</sup>

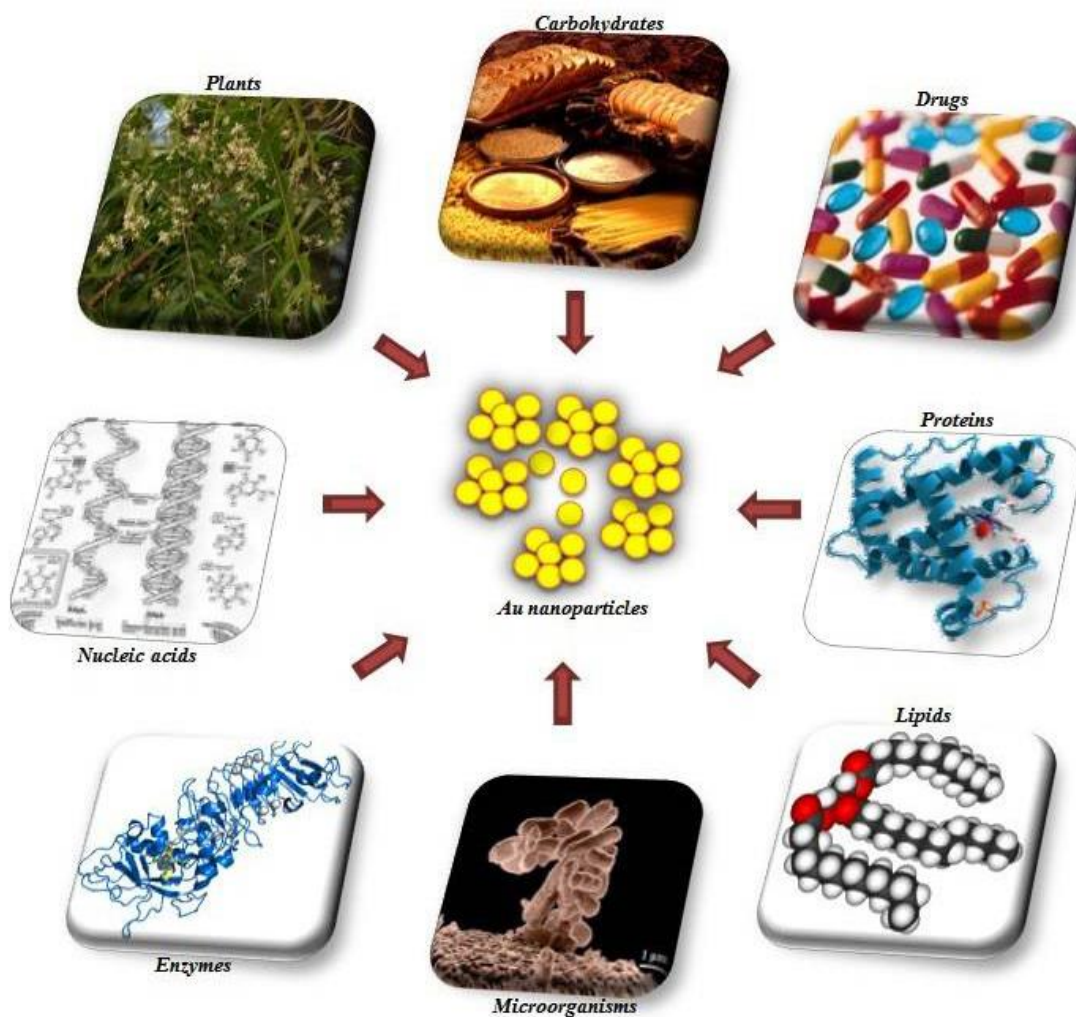


Figure 2.1: Several biological sources used in green synthesis of AuNPs.<sup>15</sup>

### 2.1.1 Turkevich method

For its simplicity of obtaining monodisperse quasi-spherical AuNPs, the most common process is that of Turkevich, presented in 1951 and refined by Frens in 1973. In particular, this green process allows the tuning of the sizes of the nanoparticles in the range of 15-25 nm, in a ruby red suspension, with the SPR peak centered at 520 nm. The protocol of the Turkevich method is the following: when the aqueous solution of  $\text{HAuCl}_4$  reaches the temperature of 90-100 °C, a rapid injection of the aqueous solution of trisodium citrate is performed. During the reaction, sodium citrate acts as a reducing and capping agent, and depending on the amount of added citrate, the pH of the  $\text{HAuCl}_4$  solution increases from ~2 to higher values. As the pH increases,  $\text{AuCl}_4^-$  ions can be hydrolyzed into different hydroxylated species,

## CHAPTER 2: SYNTHESIS OF AuNPs IN SOLUTION

---

where the  $\text{OH}^-$  groups replace the Cl atoms in  $\text{AuCl}_4^-$  ions, with a progressive decrease of the reactivity of auric precursor ions (Tab.2.1).<sup>17</sup>

When sodium citrate is added at high temperature in a water solution of  $\text{HAuCl}_4$ , is oxidized to sodium acetone dicarboxylate (SADC), while each gold precursor ion is reduced to AuCl. According to the amount of citrate, the pH of the reaction solution becomes less acid or even neutral. The coagulation of macromolecular SADC/AuCl complexes induces the formation of Au nuclei by the disproportionation of AuCl.

In the same time at high temperature, and especially at higher pH, SADC decomposes to acetone, which in turn reduces auric precursor ions to AuCl, in secondary nucleation that is minimized, in contrast, at a lower pH, where there is a fast reduction of citrate to SADC.<sup>18</sup>

The key step of nucleation and growth rates is the disproportionation of  $\text{Au}^+$  ions to  $\text{Au}^0$ . If this reaction is enough slow, there is greater control over the number of nuclei and of their growth, which leads to a temporal separation of nucleation and growth of gold nanoparticles, with a narrow size distribution according to LaMer model.<sup>19</sup>

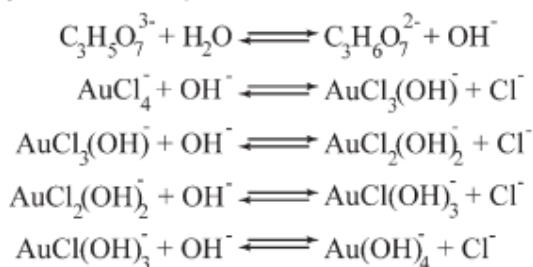
The burst nucleation and diffusional growth mechanism of Turkevich and al. is similar to the theory formulated by LaMer and Kenyon for the formation of colloidal sulfur, and it was also accepted by Frens, although it doesn't explain the dependence of nucleation rate from the temperature.<sup>20</sup>

In 1958 the results of the study of citrate method, performed with electron microscopy (EM) and UV-vis spectroscopy by Kazuyoshi Takiyama, revealed that gold nuclei quickly formed at the initial stage of the reaction, and after the nucleation, the number of particles remained constant and they grew with an autocatalytic reaction on the surface of the nanoparticles.<sup>21</sup>

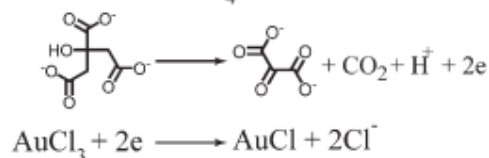
**Table 2.1: Reactivity of auric precursor ions pH dependent**

| <b>Auric precursor ions</b>    | <b>pH<sup>18</sup></b>  |
|--------------------------------|---|
| $\text{AuCl}_4^-$              | 3.3   |
| $\text{AuCl}_3(\text{OH})^-$   | 6.2   |
| $\text{AuCl}_2(\text{OH})_2^-$ | 7.1   |
| $\text{AuCl}(\text{OH})_3^-$   | 8.1   |
| $\text{Au}(\text{OH})_4^-$     | 12.9  |
| <b>Reactivity</b>              | $\text{AuCl}_4^- > \text{AuCl}_3(\text{OH})^- > \text{AuCl}_2(\text{OH})_2^- > \text{AuCl}(\text{OH})_3^- > \text{Au}(\text{OH})_4^-$ |

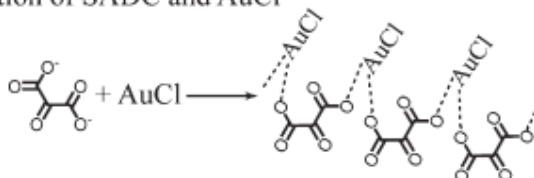
(a) Hydrolysis of HAuCl<sub>4</sub> and citrate



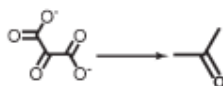
(b) Redox reaction between HAuCl<sub>4</sub> and citrate



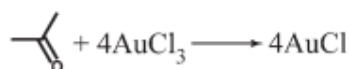
(c) Complexation of SADC and AuCl



(d) Decomposition of SADC into acetone



(e) Redox reaction between HAuCl<sub>4</sub> and acetone



(f) Disproportionation of AuCl

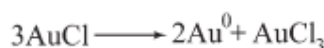


Figure 2.2: Reactions for nucleation and growth of AuNPs in the Turkevich method.<sup>18</sup>

In 1994 Zuchowsky, with his work, concluded that the mechanism of AuNPs formation initially, involves the formation of large particles containing the most of the Au<sup>0</sup> in the reaction medium, and this explains why λ<sub>max</sub> is near 590 nm before to reach the constant value of 525 nm. During the reaction, the solution changes the color from gray-bluish, to purple and finally ruby red, indicating that the AuNPs are spherical of 15-25 nm in diameter. The TEM micrographs showed the presence of both large and small nanoparticles (fig.2.3), the smallest nanoparticles seem to grow to their final size, while the large nanoparticles shrink during the course of the reaction (fig.2.3).<sup>22</sup>

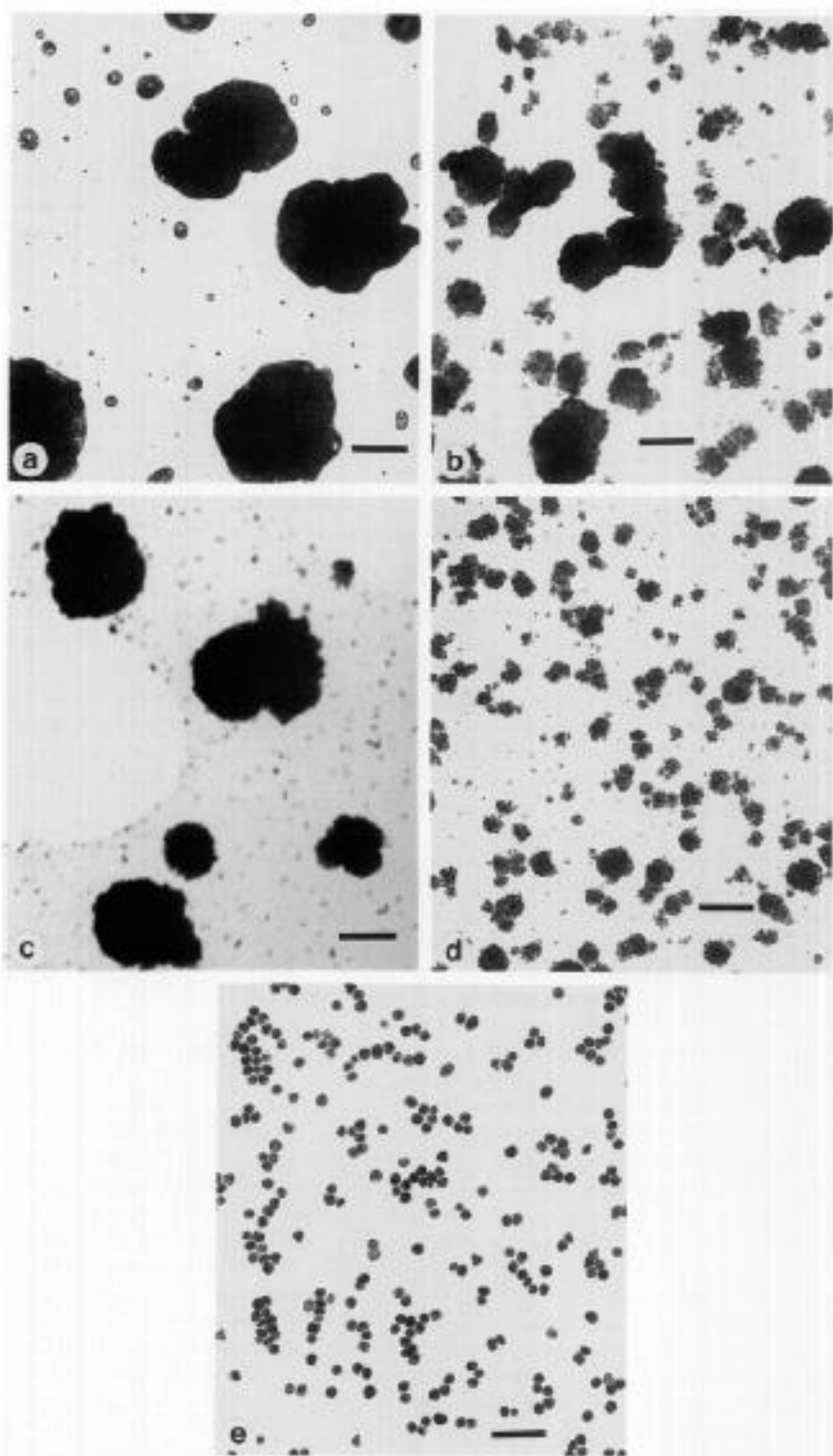


Figure 2.3: TEM images of the particles synthesized by Chow and Zukoski, (a) 10 min. (b) 30 min. (c) 60 min. (d) 120 min. (e) final particles.<sup>22</sup>

Many researchers support the hypothesis of the formation of aggregate intermediates during the Turkevich synthesis through an analysis of UV-vis and TEM data; on the contrary, according to other researchers, the formation of large

aggregates is to exclude. For example, Polte and al., monitoring in situ the particles growth, support the thesis that there is no formation of these aggregates, and the initial bluish color of the solution is due to the attachment of gold ions in electronic double layer (EDL) of the seeds, and the EDL influences the optical proprieties of AuNPs. The images of TEM of aggregates in the samples of the different steps of the reaction are some artifacts, probably due to the drying phase of the sample preparation.

Thus, the Turkevich synthesis can be described by a seed-mediated growth mechanism, in which the final number of nanoparticles corresponds to the number of seeds formed at the beginning of the synthesis.

The remaining gold ions are reduced in EDL of the seed particles, causing exclusively the growth of the existing nanoparticles and not the formation of new nanoparticles.

This growth mechanism deduced by Polte is in agreement with the work of Takiyama (1958) and consists of four steps: from the reduction of gold precursor takes place the formation of thermodynamically stable clusters of gold atoms (nuclei) before, and of the seeds particles after (radius > 1.5 nm). In the final two steps (step 3 and 4), in the EDL, occurs the reduction of ionic gold to metallic gold that grows, first slowly and then fast, on the surface of seeds, until the entire precursor is consumed (fig. 2.4).

The number and the final size of the particles are determined at the end of the second stage (reduction of 1-2% of precursor), hence the kinetics of the reduction of precursor, during the steps 3 and 4 of the growth mechanisms, doesn't affect the final size of the nanoparticles.<sup>20</sup>

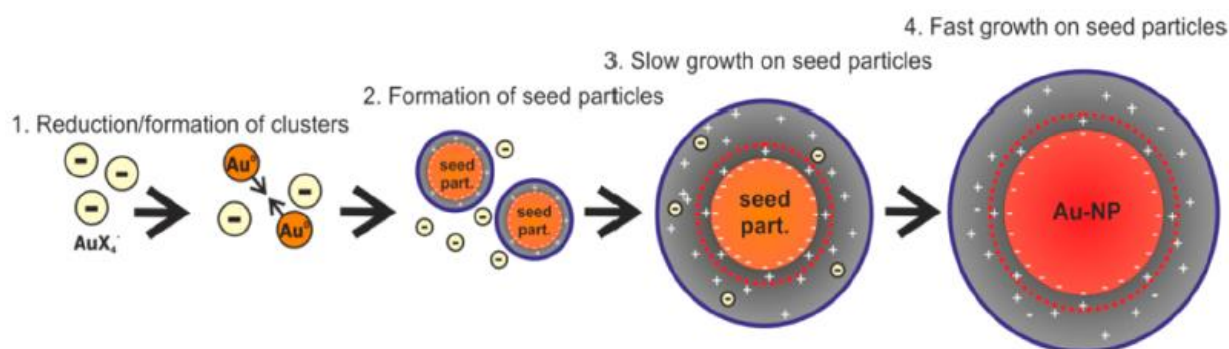


Figure 2.4: The growth mechanism of Turkevich's synthesis described by Polte.<sup>20</sup>

### 2.1.2 Colloidal stability

The growth principles of colloidal metal nanoparticles are in contrast to nucleation models because the particle size is determinate by the colloidal stability.

Usually, metal NPs are prepared via aqueous solution by reduction of metal salt in the presence of the stabilizing agent, which avoids the aggregation of NPs.<sup>23</sup>

The stabilization can be electrostatic, by adsorption of ions on the surface of NPs that cause repulsive forces, or a steric stabilization by adsorption of polymers or surfactants that confine the NPs keeping them separated.

The variation of the capping agent or its concentration can change the size of NPs. Without repulsive forces, NPs can agglomerate, aggregate or coalesce, because they are attracted to each other by Van der Waals forces.

In the electrostatic stabilization, NPs have a surface charging and one electrical double layer (EDL) forms, which causes repulsive interparticle forces.

According to the DLVO theory (Dejargan, Landau, Verwey, and Overbeek), the total interaction potential between two particles is the sum of Van der Waals and EDL forces.

In general, the colloidal stability increases with the size because the barrier aggregation is higher for larger particles than smaller particles, so the coalescence process is more likely for smaller particles.

For this reason, a model of nucleation is not essential for NPs, and the concept of colloidal stability, which depends on the interaction potential between the particles, is used to explain the growth of NPs. If the colloidal stability is sufficient to prevent further growth, the aggregation barrier is above the thermal energy of the particles  $E_{KT}$ , otherwise, the aggregation barrier is lower than the thermal energy of NPs, and the growth occurs for aggregation and subsequent coalescence (fig. 2.7). This contradicts the classical nucleation theory and in particular the LaMer theory for NPs because the formation of the primary cluster with a critical radius is irrelevant.

The critical radius  $R_{KT}$  in fig. 2.7, is the radius of the smallest particles in the final distribution: smaller particles than  $R_{KT}$  can still coalesce, while the larger particles remain stable.

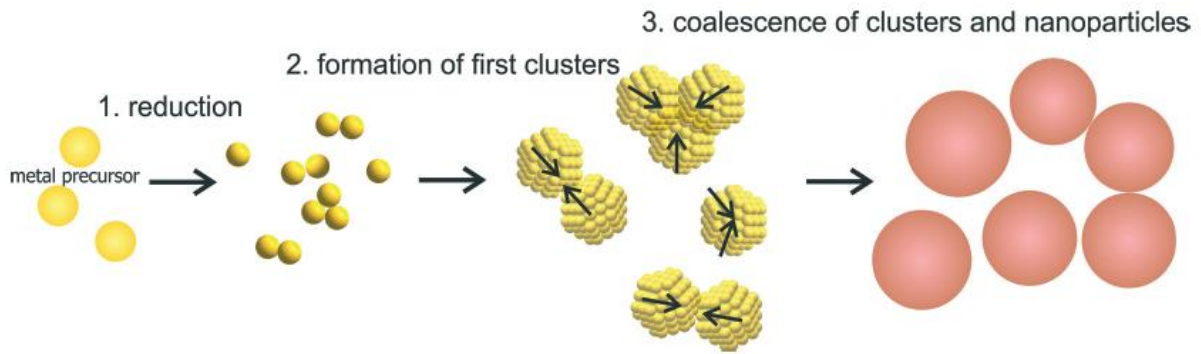


Figure 2.5: Mechanism of nanoparticle growth due to coalescence.<sup>23</sup>

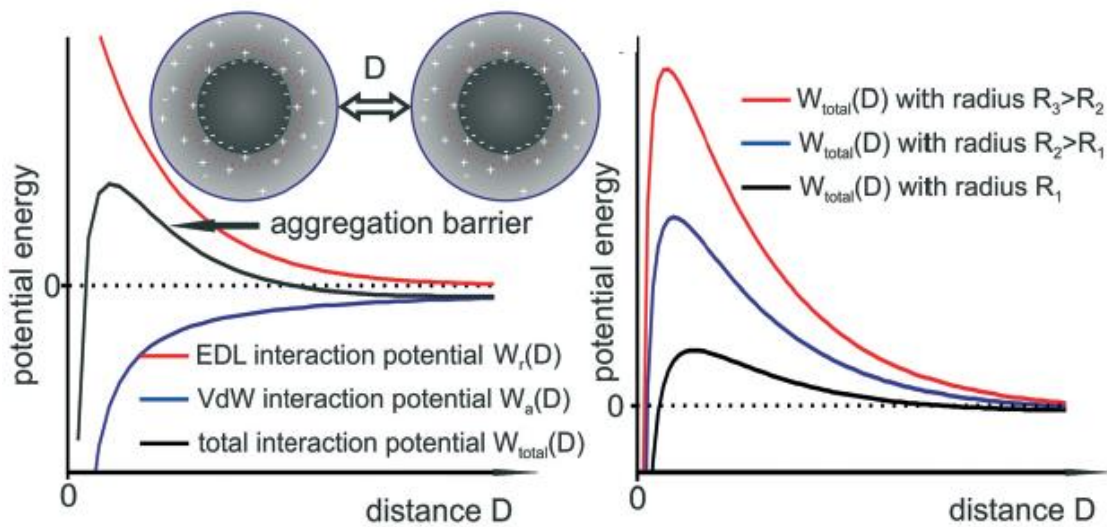


Figure 2.6: Interaction potential between two spherical particles and the dependence from the particle size.<sup>23</sup>

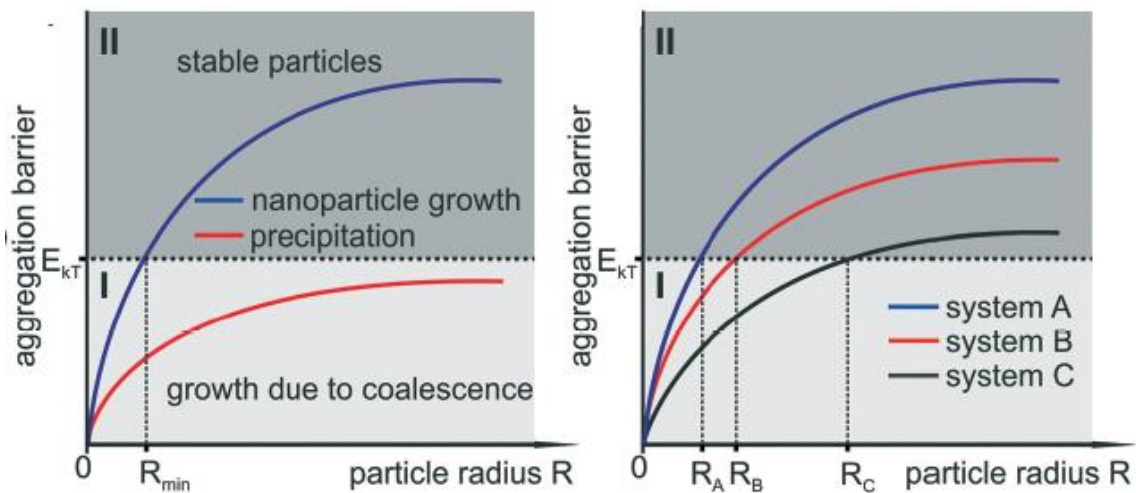


Figure 2.7: The nanoparticle growth based on the concept of colloidal stability.<sup>23</sup>

The final monodisperse system in the Turkevich method is due to two factors: reduction chemistry and colloidal stability of the seed nanoparticles.

## CHAPTER 2: SYNTHESIS OF AuNPs IN SOLUTION

During the first two steps, the reduction chemistry causes the formation of the seeds, therefore the reduction takes place on their surface, while the reduction of the precursor onto AuNPs in step 3 and 4 has no effect on the final dimensions.

The colloidal stability determines the minimum radius of metal nanoparticles at any time, and a low colloidal stability corresponds to a smaller number of seed nanoparticles with larger dimensions, if the colloidal stability is not sufficient, fewer nanoparticles with larger dimensions are formed which can precipitate.

Therefore, the Turkevich method occurs with a seed particle formation and a surface enhanced reduction with different physicochemical processes (fig.2.8), where the lack of colloidal stability is responsible for uncontrolled NPs growth or of unwanted precipitation.

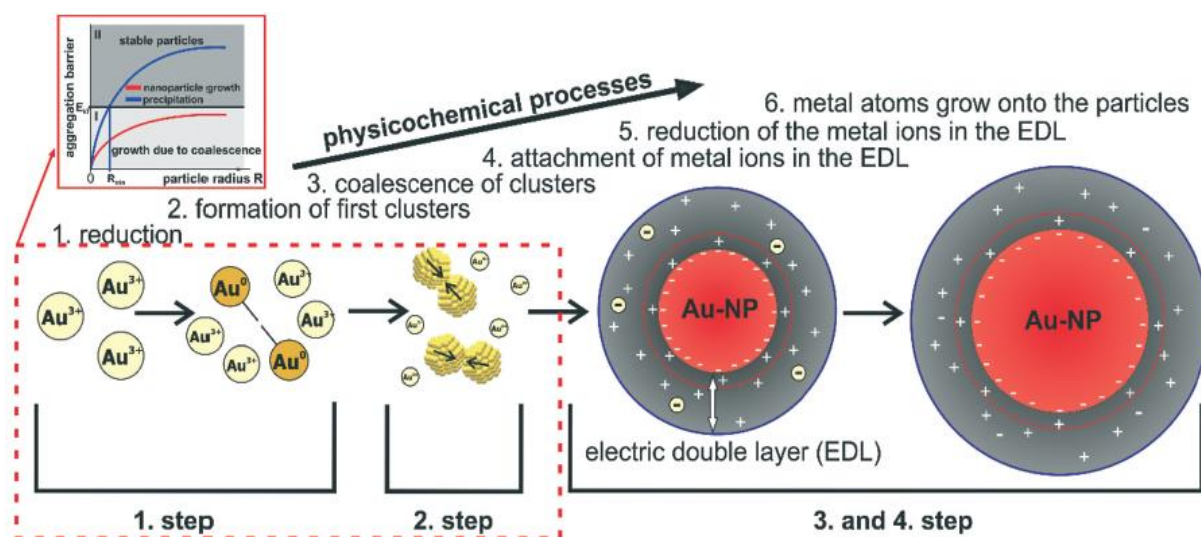


Figure 2.8: Description of Turkevich method for the synthesis of colloidal gold.<sup>23</sup>

### 2.2 Reaction parameters in the Turkevich synthesis

Many studies have been performed to understand the role of the parameters of the synthesis reaction (concentration of the reagents, pH, and temperature) on the growth mechanism of the colloidal AuNPs. The reaction conditions can influence the stability of the colloidal solution, the morphologies of the seed particles, and therefore the number and the size of the final AuNPs, on which their unique properties depend, in particular, the optical properties.

The pH of the solution affects the size, morphology, and polydispersity of the gold nanoparticles.

A higher polydispersity is predominant at  $\text{pH} < 5.0$ , while a quasi-spherical shape of AuNPs with a narrow distribution is more likely at  $\text{pH} > 6$ . In the range of  $\text{pH} 5-6$ , the shape is ellipsoidal and the aspect ratio of the nanoparticles increases with  $\text{pH}$ , achieving the maximum at  $5.0+0.5$  and decreases near  $1.0$  at  $\text{pH} 6.5$ .

The particles remain spherical in the range of  $\text{pH} 6.5-11.0$ , but at  $\text{pH} 7.0$  the size distribution is as narrow as possible, while at  $\text{pH} 7.5-11.0$  is difficult to control the action of the citrate.

The release of  $\text{H}^+$  in the solution depends on the oxidation of citrate, and therefore the  $\text{pH}$  decreases dramatically during the preparation.

For solutions prepared at lower  $\text{pH} < 5$ , the triangular and trapezoidal shapes are predominant, therefore the ellipsoidal model is not suitable anymore, and in this case, the diameter and the monodispersity of AuNPs decrease.

According to the  $\text{pH}$  of the medium, the citrate can exist in five ionized species in the solution, in different percentages, and the colloidal stability depends on the absorption of the ions citrate on the surface of nanoparticles. The charges and the absorption of ions on the surface, affect the growth and the aggregation of the NPs and therefore their size.

The charge of the citrate ions determines the electrostatic energy barrier among the NPs, in fact, it is well known that the citrate stabilizes the colloidal gold solutions and the surface curvature of colloids tends to decrease to reach a lower surface energy.

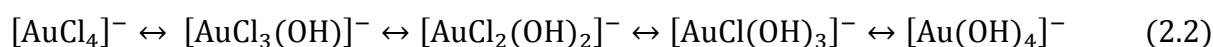
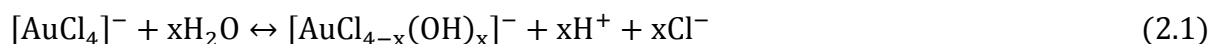
From the literature it is evident that large polyhedrons and irregular particles are formed, when in the solution, there are citrate ions with low charge (low  $\text{pH}$ ); while ellipsoids and spheroids are formed, when the charge of ions citrate is more negative than  $-1$  ( $\text{pH} > 5.5$ ).<sup>24</sup>

Hence, by modulating the  $\text{pH}$ , it is possible to promote the formation of different species of ions citrate, the surface charge, the interaction potential among nanoparticles and therefore the shape and the mean size of AuNPs:

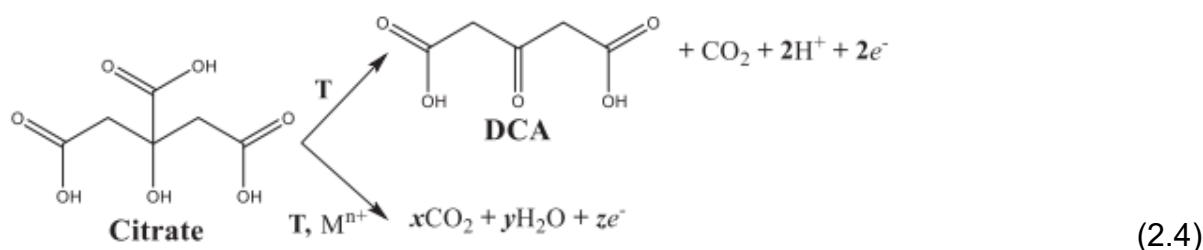
- Polyhedrons at  $\text{pH} < 5$
- Elliptical particles at intermediate  $\text{pH} 5-6$
- Spheroids at  $\text{pH} > 7.0$

## CHAPTER 2: SYNTHESIS OF AuNPs IN SOLUTION

The speciation of  $\text{Au}^{3+}$  and of citrate is shown in the fig 2.9 as a function of the pH and the equilibria of the reactions can be described in this way<sup>25</sup>:



At the same time citrate can be oxidized to dicarboxy acetone (DCA) or completely decomposed to  $\text{CO}_2$  and  $\text{H}_2\text{O}$  releasing useful electrons for the reduction of  $\text{Au}^{3+}$  to  $\text{Au}^0$  (2.4).<sup>26</sup>



DCA accelerates the reduction of  $\text{Au}^{3+}$ , but does not affect the final particle size.

The speciation of citrate depends on the pH, but also on the  $\text{Cl}^-$  concentration, because it affects the speciation of  $\text{Au}^{3+}$ , changing thereby the pH.

On acid condition, the amount of  $[\text{AuCl}_4]^-$  in the solution depends on the  $\text{Cl}^-$  concentration and this complex of Au shows a peak of absorption at 313 nm for the  $p_\sigma \rightarrow 5d_{x^2-y^2}$  ligand-metal transition.

An acidification of the  $\text{HAuCl}_4$  solution with HCl promotes the formation of a higher number of seeds in the first phase of the synthesis, since the concentration of  $[\text{AuCl}_4]^-$  increases. In particular a high concentration of  $[\text{AuCl}_4]^-$  can promote the seed formation, when there are more protonated species of citrate in the solution: in these conditions, the reduction rate of  $\text{Au}^{3+}$  to  $\text{Au}^{1+}$  to  $\text{Au}^0$  is accelerated.

The mild acid conditions (pH 4.8-6.5) promotes the formation of smaller AuNPs (5.5 nm for a pH of 5.4) where the  $\text{HCit}^{2-}$  (monoprotonated citrate) is the dominant species. The range of pH where the amount of  $\text{HCit}^{2-}$  is high corresponds to the smallest nanoparticles with the lowest polydispersity and the formation of the seeds is mainly due to the reduction of  $[\text{AuCl}_4]^-$  by  $\text{HCit}^{2-}$  (fig.2.9).

The Turkevich synthesis is lead approximately at pH between 5.4-6.8, where the formation of the seeds lasts 20s and ends with the transition of  $[\text{AuCl}_4]^-$  to  $[\text{AuCl}_{4-x}(\text{OH})_x]^-$ . The residual precursor is reduced in EDL of the seeds that form monodisperse AuNPs (*seed-mediated growth*).

## CHAPTER 2: SYNTHESIS OF AuNPs IN SOLUTION

For pH above 7, the concentration of  $\text{HCit}^{2-}$  is rather low,  $\text{Cit}^{3-}$  and  $[\text{Au}(\text{OH})_4]^-$  are the dominant species, so few seeds and large AuNPs are formed with a polydispersity of around 20% and the reduction of  $\text{Au}^{3+}$  in the EDL is hindered.<sup>25</sup>

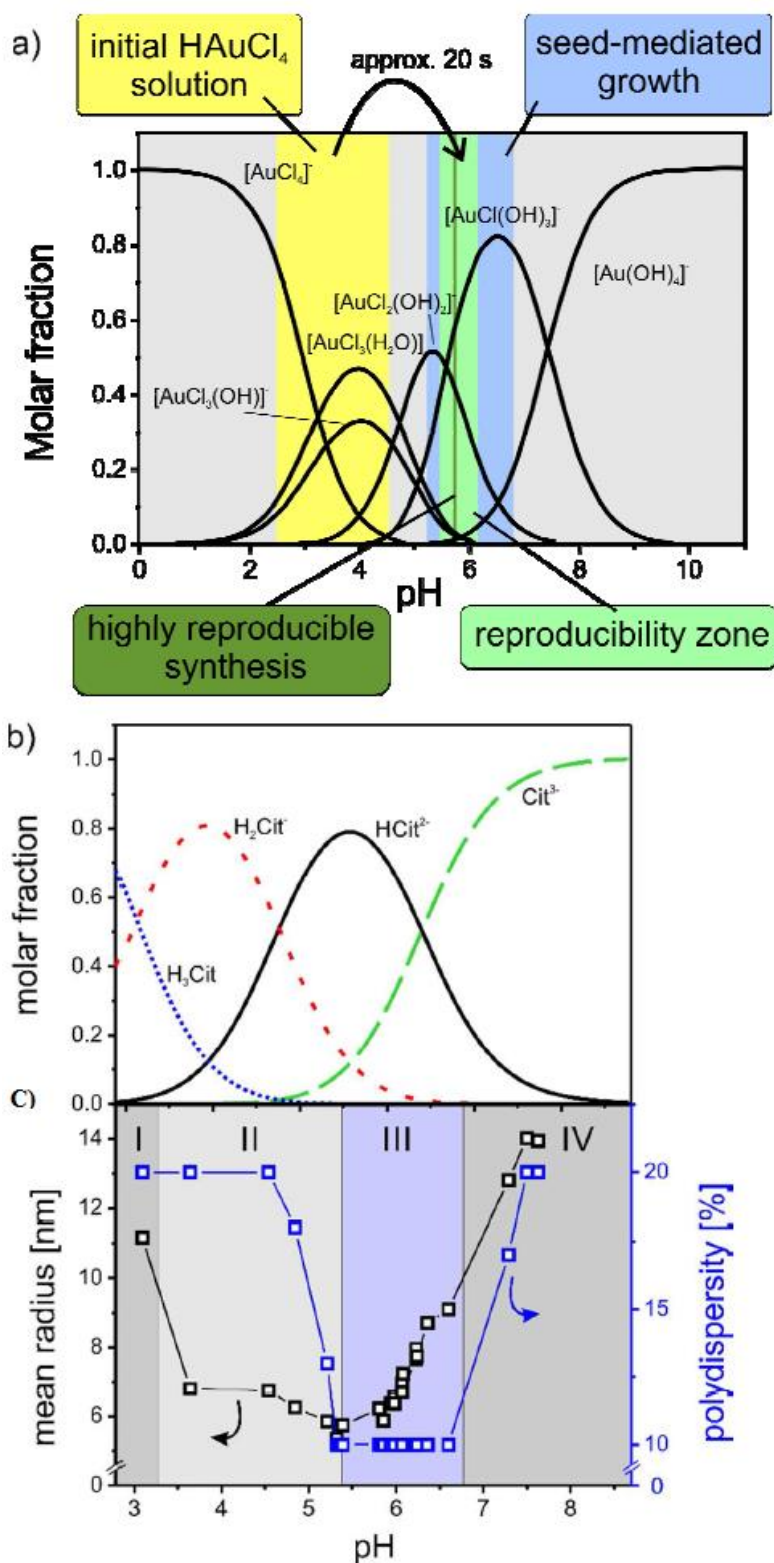


Figure 2.9: Speciation diagram of gold hydroxo-chloro complexes (a) and citrate (b), and final size and polydispersity of AuNPs obtained by standard Turchevich synthesis (c)<sup>25</sup>

## CHAPTER 2: SYNTHESIS OF AuNPs IN SOLUTION

Also for a low pH of the final solution ( $\text{pH} \leq 3$ ) the AuNPs are large and the polydispersity around 20% (fig.2.9 (c)), here the conditions are: low concentration of  $\text{HCit}^{2-}$  and a hindered transition of  $[\text{AuCl}_4]^-$  to  $[\text{AuCl}_{4-x}(\text{OH})_x]^-$ , so there isn't a separation between the formation of the seeds and their growth.

In the range of pH 3-5.4 the particles have a typical size obtained with the Turkevich method ( $r = 6-9 \text{ nm}$ ), but the polydispersity is high, because this range is a zone of transition, where the formation mechanisms of seed particle and the seed-mediated growth are not well separated.

According to the mechanism of Turkevich, after the seed formation,  $[\text{AuCl}_4]^-$  there isn't anymore in the solution and  $[\text{AuCl}_{4-x}(\text{OH})_x]^-$  complexes are reduced in the EDL of the seed particles during the seed-mediated growth, and the final AuNPs are quasi-spherical due to the size focusing effect (fig.2.10).<sup>25</sup>

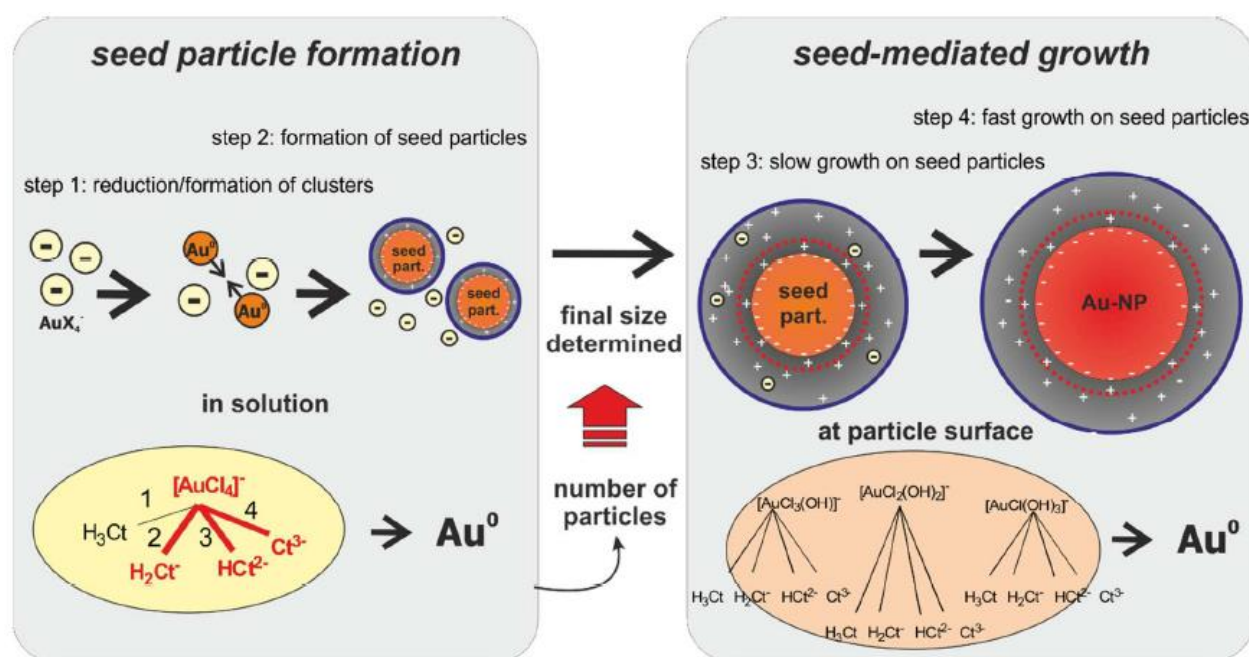


Figure 2.10: Mechanism of the Turkevich synthesis<sup>25</sup>

In theory, a range of pH where the reproducibility of the synthesis is really high, is that in which the concentration of  $\text{HCit}^{2-}$  doesn't depend strongly by little variations of pH. This range is calculated to be 5.5-6, in particular the final size of AuNPs are highly reproducible at pH around 5.9 (fig. 2.9 (a)).

For this reason, it is important to consider different parameters for the control of pH:

- Addition of  $\text{HCO}_4$ ,  $\text{HCl}$ , to  $\text{Na}_3\text{Cit}$  or  $\text{HAuCl}$  solution before the mixing

- A right ratio of Na<sub>3</sub>Cit and HAuCl<sub>4</sub>
- A right ratio of H<sub>3</sub>Cit and Na<sub>3</sub>Cit

Besides pH, the parameter that influences the kinetics of reduction of Au<sup>3+</sup> to Au<sup>0</sup> is the temperature, that has an effect on the stability of the gold complexes and thus on the initial concentration of [AuCl<sub>4</sub>]<sup>-</sup>, which can form [AuCl<sub>4-x</sub>(OH)<sub>x</sub>]<sup>-</sup> species, and can be reduced to Au<sup>0</sup>, determining the amount of monomers for the formation of seeds. This means that the temperature has an important role in the seed particle size. At higher temperature, few and larger seeds are formed because there is less [AuCl<sub>4</sub>]<sup>-</sup> and the thermal energy  $E_{KT}$  of the system increases, moving the minimum particle radius towards larger dimensions.<sup>20</sup>

During the nucleation and growth of gold nanoparticles, the reduction of Au(III) to Au(I) is the rate determining step, while the reaction of disproportionation of Au(I) to Au(0) controls the number of nuclei and their growth rate, and the Au atoms grow homogeneously on the nuclei due to the low supersaturation.<sup>27</sup>

The induction period before the nucleation, perhaps due to the formation of acetone dicarboxylic acid, a nucleating agent to form gold atoms, is the time to reach a fairly high level of concentration of Au(I) for the nucleation of the gold seeds.

During the reactions, the reduction potential of gold complexes changes, because the pH changes, as well as the reactivity of Au complexes and that of sodium citrate.

At room temperature, the redox reactions in the gold water solution are the following:



From these reduction potentials, the disproportionation of AuCl<sub>2</sub><sup>-</sup> (1) is not favorable at room temperature.<sup>28</sup>



A slow reduction of Au(III) can occur through the citrate ions (a weak reducing agent), while the number of nuclei depends on the degree of supersaturation of the solution controlled by the formation rate of Au(I), that is ensured when they are high:

- The HAuCl<sub>4</sub> concentration
- The citrate ion concentration
- The temperature



### 3 Nucleation and growth of nanoparticles in solution

#### 3.1 Homogeneous and heterogeneous nucleation

The process of nucleation consists of the nuclei or seed formation, where the seeds represent a phase transition and act as centers of crystallization. When the nucleation occurs in systems lacking crystalline matter, it is called primary nucleation, whereas when the nucleation takes place near some crystals, is indicated as secondary nucleation. Furthermore, the process of primary nucleation can be homogeneous or heterogeneous.<sup>29</sup>

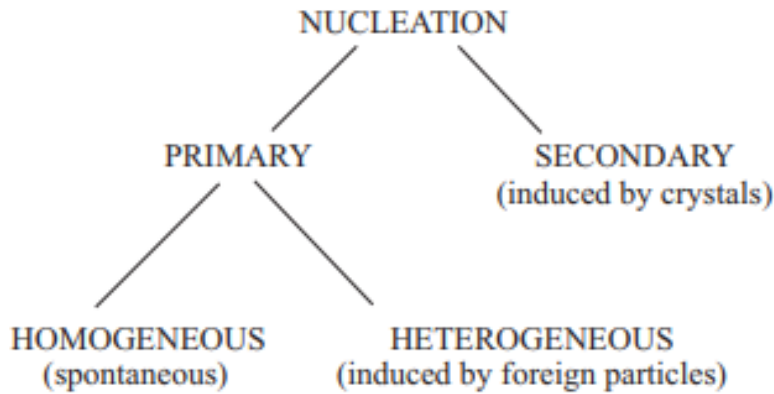


Figure 3.1: Scheme for the classification of the nucleation types

The homogeneous nucleation is a spontaneous process that occurs when the solubility of a solute in a solvent exceeds the equilibrium solubility, or when the temperature of the system reaches the phase transformation point. In these cases, a different phase is formed from the parent phase. A supersaturated solution tries to reach the minimum Gibbs free energy condition by forming the new phase with an equilibrium concentration in the solution.<sup>30</sup>

In the formation of a solid from a supersaturated solution, the Gibbs free energy per unit volume of the solid phase depends on the concentration of the solute:

$$\Delta G_v = - \frac{K_B T \ln(S)}{v} \quad (3.1)$$

Where  $k_B$  is the Boltzmann's constant,  $T$  is the temperature in K,  $S$  the supersaturation of the solution,  $v$  its molar volume.

For a spherical nucleus of radius  $r$ , the Gibbs free energy or volume free energy can be written in the following way:

$$\Delta\mu_v = (4/3) \pi r^3 \Delta G_v \quad (3.2)$$

The reduction of volume free energy, that is the driving force for the nucleation and growth of the solid phase, is accompanied by an increase of the surface energy, due to the formation of an interface.

$$\Delta\mu_s = 4\pi r^2\gamma \quad (3.3)$$

$\gamma$ =surface energy per unit area.

The total variation of the chemical potential for the nucleus formation,  $\Delta G$ , as a function of the nucleus radius, is given by:

$$\Delta G = \Delta\mu_v + \Delta\mu_s = (4/3) \pi r^3 \Delta G_v + 4\pi r^2\gamma \quad (3.4)$$

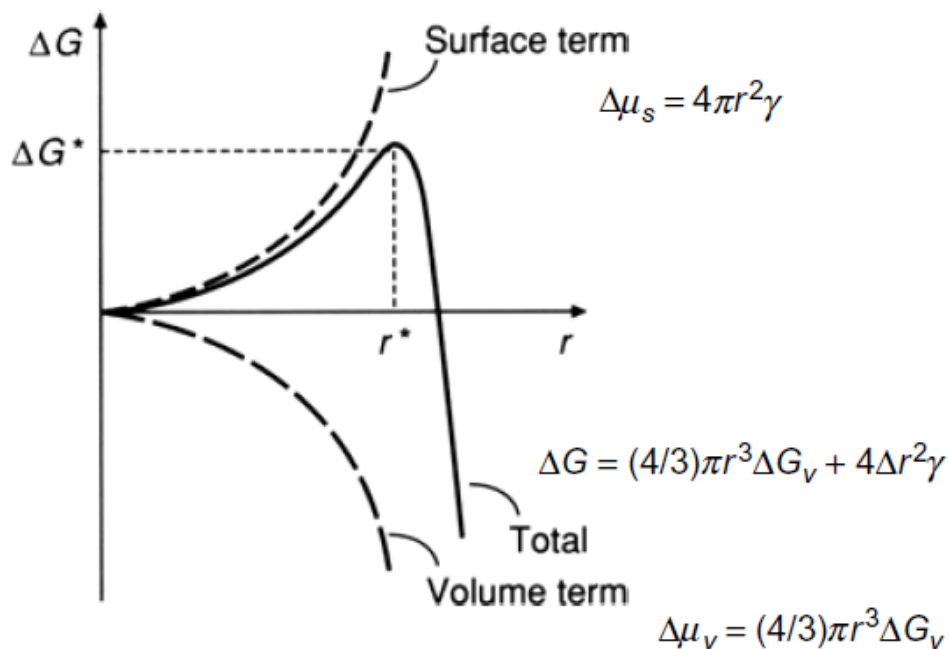


Figure 3.2: Diagram of the change of volume free energy,  $\Delta\mu_v$ , surface free energy,  $\Delta\mu_s$ , and of the total free energy,  $\Delta G$ , as a function of nucleus radius, for the nucleation process, explained by the existence of a critical nucleus radius. All the particles under this critical size dissolve in the solution; above the critical size, the particles have enough energy (they are thermodynamically stable) for the nucleation.<sup>30</sup>The critical radius and energy can be obtained by the calculation of the maximum point of the curve  $\Delta G/r$ , so for  $r = r^*$ ,  $d\Delta G/dr = 0 \rightarrow d\Delta G/dr = 8\pi r\gamma + 4\pi r^2\Delta G_v = 0$  and we have the following formula

The minimum size of a stable spherical nucleus  $r^* = -2\gamma/\Delta G_v$  (3.5)

The energy barrier for the nucleation  $\Delta G^* = 16\pi\gamma^3/3(\Delta G_v)^2 = 4\pi\gamma r^{*2}/3$  (3.6)

The nucleation rate can be described through an Arrhenius type equation:

$$\frac{dN}{dt} = A \exp\left(-\frac{\Delta G^*}{K_B T}\right) = A \exp\left(-\frac{16\pi\gamma^3 v^2}{3K_B^3 T^3 (\ln S)^2}\right) \quad (3.7)$$

Where A is the pre-exponential factor, N number of particles formed over the time t.<sup>31</sup> To reduce these two values in (3.5) and (3.6), it is possible to increase the supersaturation of the system, decreasing the temperature, and in this way, also the surface energy changes with the temperature.

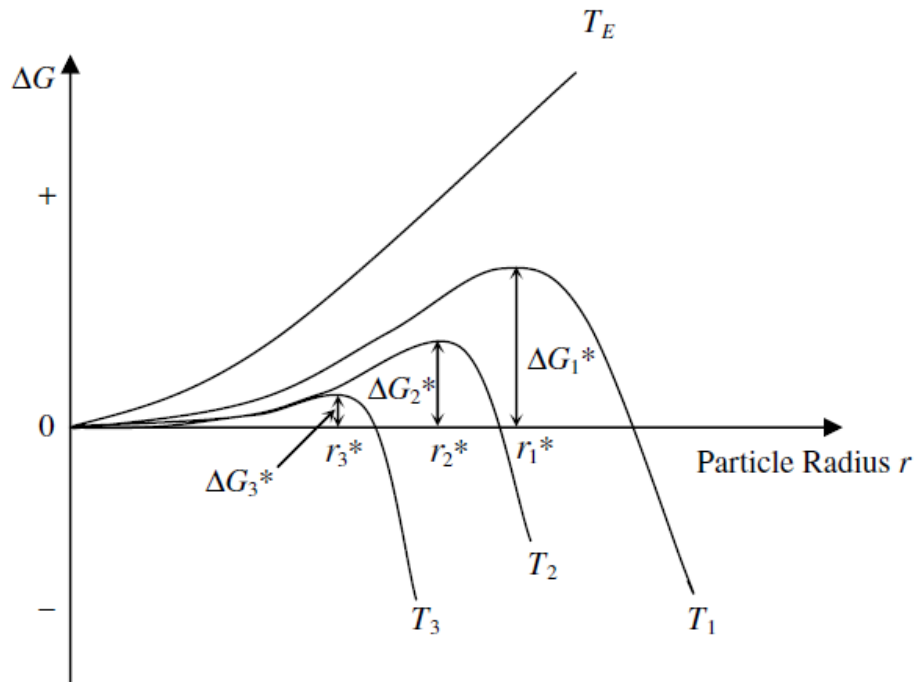


Figure 3.3: Effect of the temperature on the dimensions of thermodynamically stable spherical particles, with  $T_E > T_1 > T_2 > T_3$ , where  $T_E$  is the equilibrium temperature.<sup>30</sup>

Another way to reduce the energy barrier of the formation of nuclei and their radius is the use of different solvent, additives and the introduction of impurities, but in these cases, the nucleation is a heterogeneous nucleation, which is a more common event in the industrial field. Impurities, walls, bubbles, drops, are active centers, which lower the energy barrier for the nucleation. In this case, the nuclei of the new phase form a spherical contact angle  $\theta$  with the surface of an active center, and these

nuclei haven't anymore the spherical shape, which is instead assumed in the classical theory for the homogeneous nucleation.<sup>31</sup>

The free energy for heterogeneous nucleation is obtained from homogeneous primary nucleation multiplied for a correction term,  $\phi$ , depending on the contact angle:

$$\Delta G_{\text{crit}}^{\text{hetero}} = \phi \Delta G_{\text{crit}}^{\text{homo}} \quad (3.8)$$

$$\phi = \frac{(2 + \cos \theta)(1 - \cos \theta)^2}{4} \quad (3.9)$$

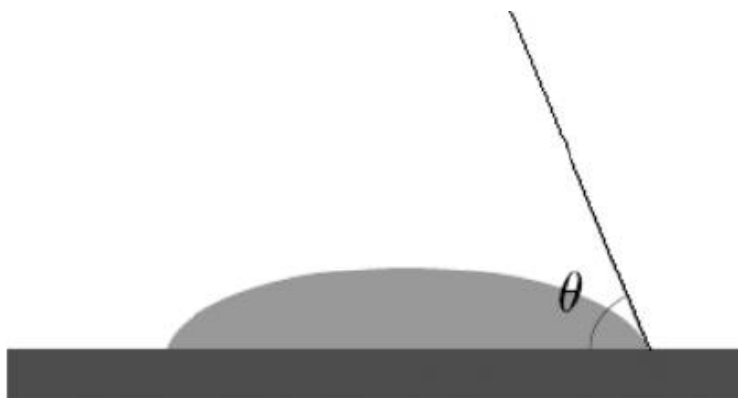


Figure 3.4: Contact angle of the nucleus with an active center during the heterogeneous nucleation.<sup>31</sup>

The classical nucleation model, as we can see from the equation (3.7), depends on the free surface energy and the molar volume of monomer, which refer to bulk solid, and the equation fits well the data for nuclei nucleation containing 10-100 molecules, so this model does not describe the formation of nanoparticles. However, from the equation (3.7) we can observe that the nucleation rate is influenced by supersaturation, temperature and free surface energy, in particular, is strongly dependent on the supersaturation level, which has an important effect on the hot injection methods for NPs synthesis.

These parameters are controllable during the synthesis of nanoparticles, in particular, according to the type and concentration of surfactant in the solution, since the free surface energy is modified and it is possible to control the nucleation rate.<sup>32</sup>

### 3.2 Diffusion controlled growth and surface reaction controlled growth

According to the classical growth theory of spherical nanoparticles in the solution, it is necessary that two things happen: the migration of monomers from the bulk solution to the nanocrystal surface and the reaction of monomers on the surface.

The first event follows the Fick's first law that for the flux of solute  $J$  through a spherical plane at a distance  $x$  from the center of nanoparticle, is written in this way:

$$J = -4 \pi x^2 D \frac{d[M]}{dx} \quad (3.10)$$

Where  $J$  is the monomers flux ( $\text{mol m}^{-2} \text{s}^{-1}$ ),  $D$  is the diffusion coefficient or diffusivity ( $\text{m}^2/\text{s}$ ),  $x$  is the distance of monomers from the center of the nanoparticle in the diffusion layer.<sup>32, 31</sup>

If  $[M]_s$  is the monomer concentration on the surface of nanocrystal ( $x = r$ ) and  $[M]_b$  the concentration of monomers in the bulk solution ( $r + \delta$ ), the total flux of monomers  $J$  on the nanocrystal surface, in the steady state, is given by the integration of  $M(x)$  from  $(r + \delta)$  to  $r$  with respect to the coordinate  $x$ :

$$J = \frac{4 \pi D r(r + \delta)}{\delta} ([M]_b - [M]_s) \quad (3.11)$$

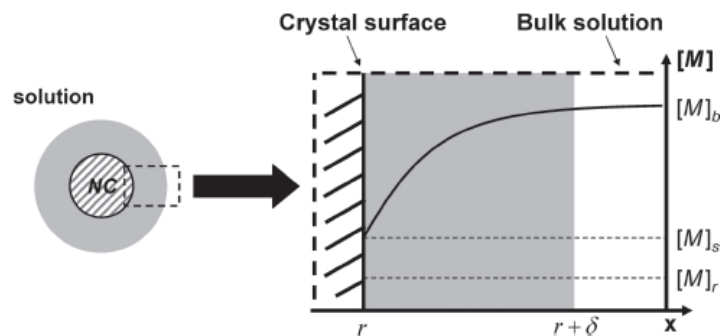


Figure 3.5: Microscopic (left) and macroscopic (right) views of the diffusion layer structure, where  $M_b$  is the concentration of solute in the bulk solution  $M_s$  is the concentration of the solute at the solid/liquid interface, and  $M_r$  is the solubility of the spherical particle of radius  $r$ .<sup>32, 33</sup>

For the surface reaction controlled growth mode exists a similar equation, where the rate constant of surface reaction “ $k$ ” of the solute on the particle surface doesn't depend on the particle size, but on the local point, where monomer and the surface of the particle enter in contact:

$$J = 4 \pi r^2 K (M_s - M_r) \quad (3.12)$$

Hence, there can be two limiting factors, the diffusion, and the surface reaction: if the diffusion controls the growth, the rate of particles radius change is:

$$\text{diffusion - controlled growth} \quad \frac{dr}{dt} = \frac{Dv}{r} (M_b - M_r) \quad (3.13)$$

With  $v$  molar volume of the solid.

If the growth is determined by surface reaction, the particle size changes can be described as:

$$\text{reaction - controlled growth} \quad \frac{dr}{dt} = kv (M_b - M_r) \quad (3.14)$$

If the growth process of NPs is neither diffusion nor surface reaction controlled, the equation of the radius change over the time is:

$$\frac{dr}{dt} = \frac{Dv(M_b - M_r)}{r + D/k} \quad (3.13)$$

Therefore, in the diffusion-controlled growth, the rate of the change of the radius is inversely proportional to the particle radius, while in the reaction-controlled growth, the rate is independent of the radius.

From the equation (3.13) it is interesting to note that as the mean particle radius decreases, the diffusion-controlled growth changes into the reaction controlled growth when  $kr$  is smaller than  $D$ .

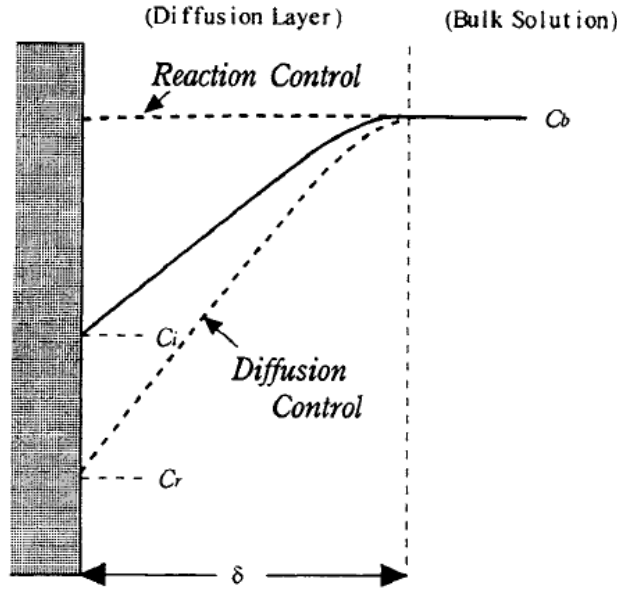


Figure 3.6: The solute concentration profiles of diffusion-controlled and reaction-controlled growth modes.<sup>33</sup>

The solubility of spherical nanoparticles,  $M_r$ , is a function of particle radius according to the Gibbs-Thomson relation, and the effect of Gibbs Thomson is important for particle size very small:

$$M_r = M_0 \exp\left(\frac{2\gamma v}{rRT}\right) \approx M_0 \left(1 + \frac{2\gamma v}{rRT}\right) \quad (3.14)$$

Where  $M_r$  and  $M_0$  are the solubilities of a particle of radius  $r$  and of the bulk solid respectively;  $\Delta\mu = \frac{2\gamma v}{r}$  is the extra chemical potential of a spherical particle, and the coefficient  $\frac{2\gamma v}{rRT}$  is called capillarity length, where  $\gamma$  is the surface tension.

The approximation for the solubility of the particles in eq. (3.14) is true if  $\frac{2\gamma v}{rRT} < 1$ .

The general expression of the particle radius evolution, from the eq. (3.13) and (3.14), can be described by the following expression:

$$\frac{dr^*}{d\tau} = \frac{S - \exp\left[\frac{1}{r^*}\right]}{r^* + K \exp\left[\frac{\alpha}{r^*}\right]} \quad (3.15)$$

The parameters are:

$$\text{dimensionless radius} \quad r^* = \frac{RT}{2\gamma v} r \quad (3.16)$$

$$\text{dimensionless time} \quad \tau = \frac{R^2 T^2 D M_0}{4\gamma^2 v} t \quad (3.17)$$

$$\text{Damköhler number} \quad K = \frac{RT D}{2\gamma v k} \quad (3.18)$$

$$\text{dimensionless supersaturation of the monomer in solution} \quad S = \frac{[M]_b}{M_0} \quad (3.19)$$

$\alpha$  is the transfer coefficient of activated complex ( $0 \leq \alpha \leq 1$ );  $r^*$  is the particle radius in equilibrium within the bulk solution. According to the value of Damköhler number, the growth is a diffusion controlled process ( $K \ll 1$ ) or a surface reaction controlled process ( $K \gg 1$ ).<sup>33</sup>

The linear growth rate of the diffusion controlled growth can be rewritten as:

$$\frac{dr}{dt} = \frac{K_D}{r} \left( \frac{1}{r^*} - \frac{1}{r} \right) \quad (3.20)$$

Where

$$K_D = \frac{2\gamma D v^2 M_0}{RT} \quad (3.21)$$

In this case, the change of standard deviation  $\Delta r$  in the function of the equilibrium radius, for narrow size distribution, is given by:

$$\frac{d\Delta r}{dt} = \frac{K_D \Delta r}{\bar{r}^2} \left( \frac{2}{\bar{r}} - \frac{1}{r^*} \right) \quad (3.22)$$

$\bar{r}$  is the mean particle radius.

- If  $\frac{\bar{r}}{r^*} < 2$ , (low supersaturation),  $\frac{d\Delta r}{dt} > 0$ ,  $\Delta r$  increases and the distribution is broader.
- If  $\frac{\bar{r}}{r^*} \geq 2$ , (supersaturation enough high),  $\frac{d\Delta r}{dt} < 0$ ,  $\Delta r$  decreases and the distribution is narrow.

Similarly, the equation of surface reaction controlled growth can be rewritten as:

$$\frac{dr}{dt} = \frac{K_R}{r} \left( \frac{1}{r^*} - \frac{1}{r} \right) \quad (3.23)$$

Where

$$K_R = \frac{2\gamma k v^2 M_0}{RT} \quad (3.24)$$

In the same way  $\frac{d\Delta r}{dt}$  is given by:

$$\frac{d\Delta r}{dt} = \frac{K_R \Delta r}{\bar{r}^2} \quad (3.25)$$

From the eq. (3.25) is evident that,  $\forall \bar{r}$ , the standard deviation is  $\frac{d\Delta r}{dt} > 0$ , hence, the size distribution is always broad when the surface reaction dominates, and this effect cannot be modified increasing the supersaturation, because in this case, there isn't the dependence between  $\frac{d\Delta r}{dt}$  and  $r^*$ .

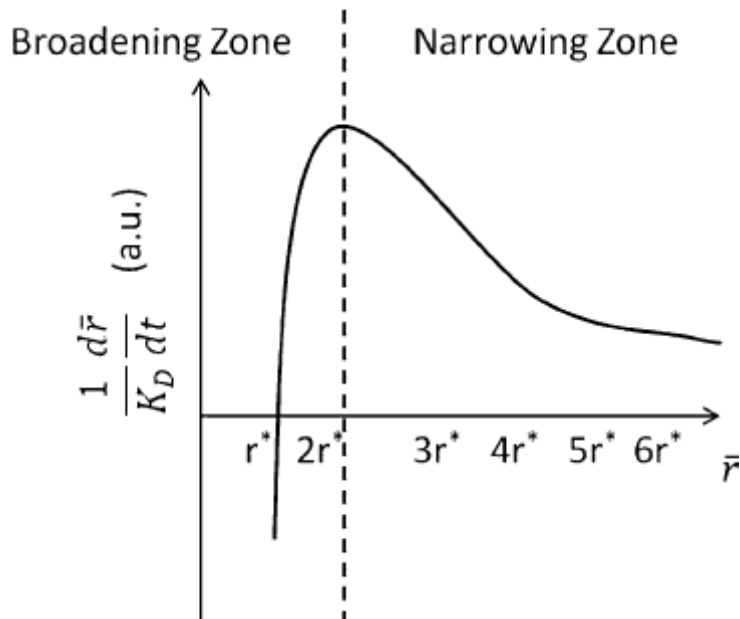


Figure 3.7:  $\frac{1}{K_D} \frac{d\bar{r}}{dt}$  vs  $\bar{r}$  for diffusion controlled growth with an infinite diffusion layer.<sup>31</sup>

As it is shown in the fig. 3.7, also in the diffusion controlled growth mode, the size distribution can be broad, when the mean radius is  $r^* < \bar{r} < 2r^*$ ; while for particles very large, the distribution is constant. In these two regimes, it is not possible to distinguish the two growth mechanisms.<sup>33</sup>

### 3.3 Mechanisms of nucleation and growth

In this section, a brief description of the theories postulated over time will be provided to explain the nucleation and growth of nanoparticles in solution.<sup>31</sup>

#### 3.3.1 LaMer model

This model, was born in the 1950s to explain the growth of monodisperse sulfur colloids and can be described through three steps, using the plot of monomers concentration versus time, where the monomers are unstable species dissolved in a solution that can easily form or attach particles.

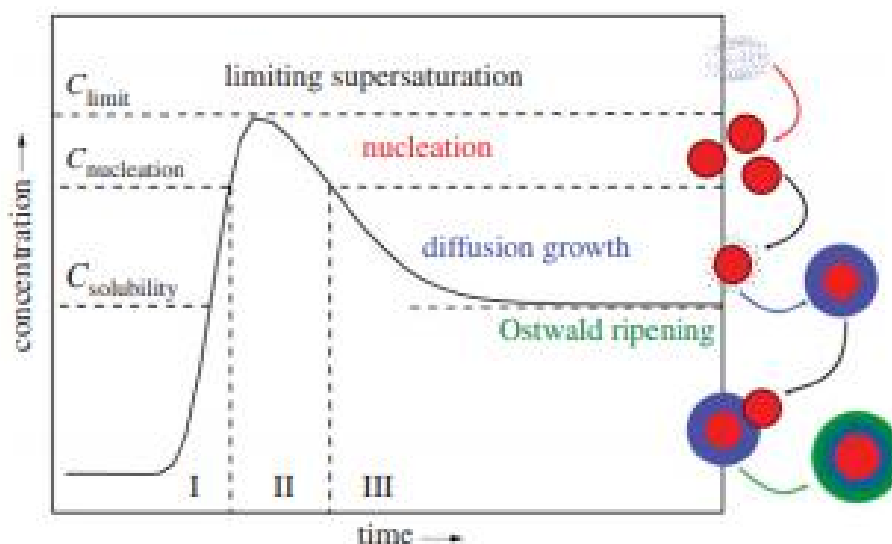


Figure 3.8: The LaMer model of nucleation and growth nanoparticles.<sup>34</sup>

The LaMer model is the first mechanism to predict that the separation of the nucleation and growth in time is the key to obtain a near-monodisperse size distribution during the synthesis of nanoparticles, even if the model can be correct or not according to the cases. Dealing with the metal nanocrystal synthesis, the concentration of metal atoms increases until a point of supersaturation, where the atoms aggregate into clusters. While the decomposition of the precursor lowers its concentration in solution, the stable nuclei form and grow in an accelerated manner and the concentration of metal atoms drops. If the growth of nuclei is very fast and the concentration of atoms decreases below the limit of supersaturation, new nuclei don't form anymore. The metal atoms supplied by the consumption of the precursor

make to grow the nuclei in nanocrystals until an equilibrium is reached between the atoms on the surface of nanocrystals and those that are in solution. In addition to diffusion growth via atomic addition, the nuclei and nanocrystals can also agglomerate into larger objects (Ostwald ripening).<sup>34,35</sup>

Following the plot in fig.3.8, the LaMer model can be described in these three passages:

- I. **Pre-nucleation:** the concentration of free monomers in solution grows up rapidly, reaching a concentration level ( $C_{\text{solubility}}$ ) at which the homogeneous nucleation is possible but the kinetics is infinite.
- II. **Rapid self-nucleation:** the saturation of the solution is so high ( $C_{\text{nucleation}}$ ) that the system reaches the activation energy for the burst nucleation with an important reduction of the concentration of free monomers in solution. When the concentration of solute reaches again the critical level the nucleation ends (homogeneous nucleation).
- III. **Crystallization:** the stable nuclei formed (seeds) grow into nanocrystals, in the absence of renucleation, through the diffusion of monomers in solution towards nanocrystals surface (heterogeneous nucleation/growth).<sup>23</sup>  
The particle growth ends as soon as the concentration of monomers reaches the solubility of the bulk solid.

In reality, the growth of NPs can proceed in different ways:

- via addition of monomers from solution to the surface of nanocrystals.
- Ostwald ripening, where large nuclei grow at the expense of the small nuclei, which redissolve and deposit on the larger nuclei, due to the high solubility and the surface energy of smaller nanoparticles.
- Digestive ripening: is the inverse of Ostwald ripening, the smallest nanoparticles in solution grow at the expense of the larger nanoparticles.
- Intraparticle growth occurs when there isn't diffusion of monomers in the solution, because the surface energy of NPs is similar to the bulk solution: there is only a diffusion of monomers along the surface of the nanomaterial, from the facets of high energy towards the facets at low energy.
- Coalescence, in which nanoparticles enter into contact and fuse.
- Orientated attachment: it's very similar to the coalescence, the difference is that, while in the coalescence there isn't a preferential attachment; for the

orientated attachment there is a preferential crystallization at the grain boundaries, with a perfect orientation of the crystalline planes.

### 3.3.2 Finke and Watzky model

There are many articles that describe the synthesis of monodispersed AuNPs in solution, but the kinetic process isn't yet well known and this aspect, as well as the knowledge of the mechanism of AuNPs synthesis, is fundamental to have the full control of the size and shape of NPs.

Colloidal metals formation is a two-stage process, where the nuclei formation is followed by their growth and these processes depend on the kinetic of reaction between the reagents and on the diffusion of metal atoms.

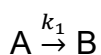
La Mer explained the NPs formation with a burst nucleation due to a supersaturation of solution followed by a rapid growth by diffusion of monomers.

According to the observations of Turkevich et al., abandoned the classical description for the synthesis of AuNPs, an incubation period was necessary for the reduction of the tetrachloroauric acid, followed by an increase of the number of nuclei and then the growth of these nuclei, whose rate decreases in the time.

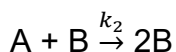
The Turkevich's observations are of fundamental importance in the synthesis of metal nanoparticles, but they don't provide any kinetic equation to extract the rate constants of the reaction process.<sup>36</sup>

Finke and Watzky (1997) provided a kinetic model for the mechanism of NPs formation that consists of two steps: a slow, continuous and homogeneous nucleation (process in contrast with the La Mer's burst nucleation), followed by a fast autocatalytic surface growth. The model can be described, by two pseudo-elementary reactions of first and second order respectively.

The nucleation process with rate constant  $k_1$ :



The autocatalytic growth with rate constant  $k_2$ :



A is the precursor and B is the surface of the growing cluster.

From the integration of the kinetic equation (3.25), we obtain the dependence of the concentration on time (3.26).

$$-d[A]/dt = +d[B]/dt = k_1[A] + k_2[A][B] \quad (3.25)$$

$$[A]_t = \frac{\frac{k_1}{k_2} + [A]_0}{1 + \frac{k_1}{k_2[A]_0} * \exp(k_1 + k_2[A]_0)t} \quad (3.26)$$

Where  $[A]_0$  is the initial metal precursor concentration,  $k_1$  and  $k_2$  are the rate constants. This model seems to fit well with many systems such as iridium, platinum and rhodium.<sup>37,31</sup>

The so-called redox-crystallization model (R-C model) for AuNPs is similar to this model. The Abs-t profile obtained by Yao Zhou et al. in 2013, by recording the absorbance of SPR of gold nanoparticles in situ, had a sigmoidal shape, with an induction stage (I), a growth stage (II) and a saturation stage(III). By investigating the UV-vis spectra in situ, the kinetic data were described in terms of a redox-crystallization model for a quantitative analysis of the nucleation and growth of spherical AuNPs.

This model can be described according to this scheme<sup>38</sup>:



(F-1) represents the existence of free gold atoms in solution because of the reduction of the gold precursor,  $M^n$ , by reducing agent (R), with an equilibrium constant  $k_c$ .

(F-2) is the crystallization of free gold atoms dissolved in solution,  $M_l^0$ , which goes in solid phase,  $M_s^0$ , thus this equation is a phase transformation, and represents the nucleation.

(F-3) is the growth of nuclei through the reaction of surface active site  $s^*$  with gold atoms in solution.

$k_{01}$  and  $k_{02}$  are the nucleation and growth rate constants respectively.

From the three pseudo-elementary reactions, we can obtain the crystallization rate (3.28):

$$[M_l^0] = k_c[R][M^n] \quad (3.27)$$

$$\frac{d[M_s^0]}{dt} = k_{01}[M_l^0] + k_{02}[s^*][M_l^0] \quad (3.28)$$

$$\text{With } [s^*] = \frac{3M_{Au}}{\rho_{Au}\bar{r}}[M_s^0] = \varepsilon[M_s^0] \quad (3.29)$$

$\varepsilon$  is a constant and  $M_{Au}$  is the molar mass of gold,  $\rho_{Au}$  the density, and  $\bar{r}$  the equivalent average radius of AuNPs.

From the mass conservation law, the initial concentration of gold precursor  $[M^n]_0$ , can be written as:

$$[M^n]_0 = [M^n] + [M_l^0] + [M_s^0] \quad (3.30)$$

From the equation (3.28) and (3.30) the crystallization fraction results to be:

$$x = \frac{M_s^0}{[M^n]_0} = 1 - \frac{k_{02}\varepsilon[M^n]_0 + k_{01}}{k_{02}\varepsilon[M^n]_0 + k_{01}e^{\alpha(k_{01}+k_{02}\varepsilon[M^n]_0)t}} \quad (3.31)$$

Where  $\alpha = k_cR/(k_cR + 1)$

If  $K_1 = \alpha k_{01}$  is the apparent overall nucleation rate constant and  $K_2 = \alpha\varepsilon[M^n]_0 k_{02}$  the apparent overall growth rate constant with measurement units  $s^{-1}$ , the crystallization fraction becomes:

$$x = 1 - \frac{k_1 + k_2}{k_2 + k_1 e^{(k_1+k_2)t}} \quad (3.32)$$

It is possible to fit Abs/t plots by UV-vis in situ, with R-C model, transforming the equation (3.32) into (3.33):

$$A_t = A_{max} \left( 1 - \frac{k_1 + k_2}{k_2 + k_1 e^{(k_1+k_2)t}} \right) \quad (3.33)$$

Where  $A_t$  is the absorbance of SPR at t time and  $A_{max}$  is the maximum absorbance at the end of the synthesis.

The mathematical expression of the reduction-crystallization model for GNPs is equal to the mathematical formula of Finke-Watzky model.<sup>37, 39</sup>

## 4 Analysis techniques

The analysis techniques employed for the characterization of AuNPs are the measurements in situ of pH of the solution and the reduction potential (Eh) of gold at constant temperature, and at the same time, the UV-vis spectra evolution, in terms of absorbance are monitored and recorded, during all the formation process of colloidal gold in water solution. From these analyses we obtain some plots of pH and Eh vs time and we can calculate the extinction in the UV-vis range in the time.

The software to record and read the values of T, pH and reduction potential is Tiamo, while for the evolution of UV-vis spectra is Ocean view.

At the end of the synthesis, when the pH and reduction potential don't change anymore, the reaction is stopped, and a sample of the solution obtained is used for ex situ analysis at room temperature. The TEM images and UV-vis spectrum are performed for an analysis of the morphology of the AuNPs, and the control of stability of the colloidal solution respectively.

### 4.1 Set up for the synthesis of AuNPs in water solution

The set up, in the laboratory, for the synthesis of colloidal gold solution and the kinetic characterization in situ, of the parameters of the reaction, Eh, pH, T and the evolution of optical properties, consists of different instruments.

A thermostatic bath to bring the reactor to temperature, where the synthesis reaction takes place. A glass jacketed reaction vessel as a reactor put on a stirrer and containing a stir bar for the shaking of the solution during the entire time of the synthesis.

Three electrodes, all immersed in the solution in the reactor: one for the measurement of Eh, one for pH (and this electrode records also the temperature), and one electrode for UV-vis spectra.

A detector device for the working of the electrodes of pH, Eh, and the stirrer, and the connection of the device to a PC through a USB connection. A UV-vis source

connected to the probe through an optical fiber, and an optical fiber connection from the probe to a miniature spectrometer connected to the PC by means of a USB connection.

The monitor of the PC, coupled to another monitor, allows to follow, in real time, during the entire synthesis process, the changes of the parameters, Eh, pH and T, in the second monitor, and the evolution of the UV-vis spectrum in the PC, thanks, over all, to two software Tiamo and Ocean view.



Figure 4.1: Setup for synthesis and characterization in situ of colloidal gold

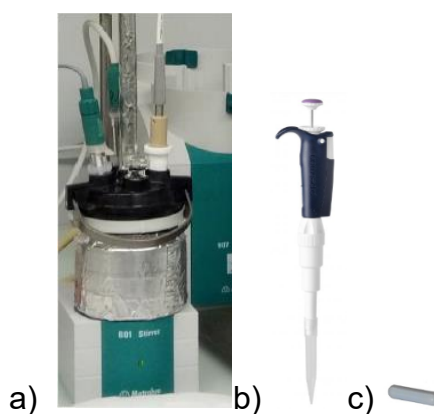


Figure 4.2: a) Glass jacketed vessel reactor with three electrodes for measurement of Eh, pH&T, UV-vis spectrum upon the magnetic stirrer. b) Pipetman L P500L, 500-5000 $\mu$ L for the hot injection  
c) A magnetic stir bar 30.0 mm x 6 mm.

## 4.2 Measurements in-situ

During these measurements, the thermostatic bath employed to bring the water solutions to the desired temperature, is a Thermo Fisher Scientific Haake S7.

The first step is the heating of the water Milli Q in the reactor as reference sample for the analysis UV-vis. The second step is the heating of the water solution of  $\text{HAuCl}_4$  and the third step is the injection of the reducing and stabilizer agent with a pipette in the hot solution. The solutions in the reactor are always under stirring by using a magnetic stir bar in the glass vessel positioned over a magnetic stirrer (fig.4.2).



Figure 4.3: Thermo Fisher Scientific bath Haake S7

### 4.2.1 Measurement of reduction potential (Eh)



**Figure 4.4: Metrohm combined gold ring electrode with a ceramic pin diaphragm order number 6.0452.100.**

The reduction potential of the samples was measured using a Metrohm combined redox electrode consisting of an Au-ring indicator electrode coupled with an Ag/AgCl reference electrode (3M KCl filling solution, that is, the wire of the reference electrode is immersed in potassiumchloride (KCl) solution of 3M concentration) This instrument is stored in deionized water and it is well suited for redox titrations when the pH varies.

### 4.2.2 Measurements of pH and temperature



**Figure 4.5: Metrohm combined pH electrode with integrated Pt1000 temperature sensor and fixed cable (1.2 m, diameter banana plug 2 mm). Order number 6.0258.010.**

This electrode is suitable for the measurement of pH in difficult sample (e.g. viscous or alkaline), is resistant to high temperatures, to the contaminations and it is suitable for long term of measurements. The reference electrolyte is KCl 3M and the electrode is stored in the storage solution. Thanks to a Pt integrated sensor, it allows also the measurement of the temperature, during all the reaction.

### Titrando 907



Figure 4.6: Front 907 Titrando.<sup>40</sup>

Titrando 907 is a device that works via Touch Control with a touch sensitive screen or by a computer with a corresponding software, and has been used for the pH, temperature and potentiometric voltage measurements in situ by means of the electrodes above described and immersed in the solution of interest.

Titrando 907 has been connected to the PC via a USB connection and recognized by the Tiamo software.<sup>40</sup> In the fig. 4.9 is visible also the magnetic stirrer used during the synthesis of colloidal gold, a device connected to the Titrado 907.

### 4.2.3 UV-vis spectra evolution

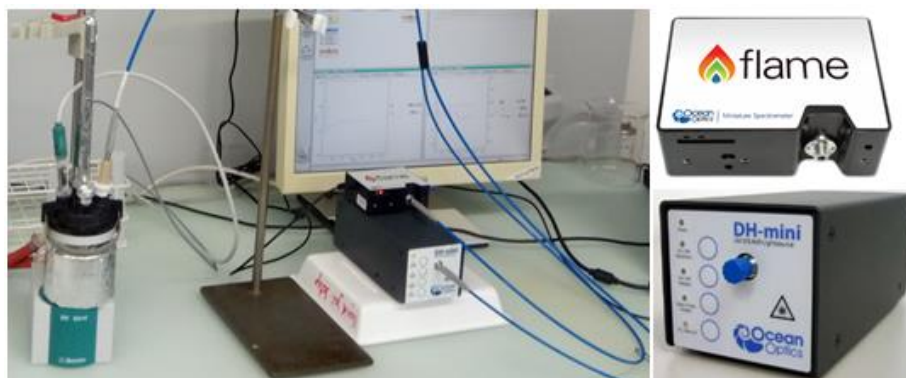


Figure 4.7: Set up for recording the evolution of the UV-vis spectra of colloidal gold during the synthesis: a DH-mini-2-GS UV-vis-NIR light source<sup>41</sup>, a miniature flame spectrometer USB2000+XR1<sup>42</sup>, an ocean optics bifurcated fiber optic, and an ocean optics transmission dip probe T300 serie immersed in the solution contained in the glass vessel.

A transmission dip probe T300 ocean optics series is coupled to a spectrometer and a light source to measure the absorbance in the solution in real time. The light reaches the solution through an optical fiber and one open path (1cmx1cm) in the final part of the stainless steel probe, where the solution is free to flow and the probe measure both transmitted and backscattered light. Here the light is reflected by a mirror and goes to the spectrometer through the receiving optical fiber.<sup>43</sup>

The probe measures both absorbed and backscattered light. Indeed, in the medium both scattering and absorption occur and their sum is known as extinction.

The absorbance is:

$$A(\lambda) = -\text{Log}(I_{\text{sam}}/I_{\text{ref}})$$

$I_{\text{sam}}/I_{\text{ref}}$  is the ratio between the intensity of the light, that goes through the sample solution, and the intensity of the light when the vessel is full of only water that is the solvent.<sup>44</sup>

For more precise optical measurements the reference and the dark spectra are necessary, and the above equation becomes:

$$A(\lambda) = -\text{Log}((I_{\text{sam}} - I_{\text{dark}})/(I_{\text{ref}} - I_{\text{dark}}))$$

Where  $I_{\text{dark}}$  is the intensity of the light recorded by the spectrometer when the source of the light is blocked.

In the same way it is possible to define the transmittance  $T(\lambda)$ :

$$T(\lambda) = (I_{\text{sam}}/I_{\text{ref}}) * 100\% \text{ and with the dark spectra becomes:}$$

$$T(\lambda) = ((I_{\text{sam}} - I_{\text{dark}})/(I_{\text{ref}} - I_{\text{dark}})) * 100\%$$



Figure 4.8: TP300 Transmission dip probe by ocean optics for UV-vis-NIR with 1 cm optical path length.

### 4.3 Measurements ex-situ

#### 4.3.1 TEM

For images at high resolution has been used a HRTEM Jeol JEM-2010 at 200 kV and the samples were prepared by drying 10 $\mu$ L of solutions deposited on amorphous carbon-coated copper grids.

The images by TEM were analyzed by image J software to measure the major and minor diameter of 100 nanoparticles for each solution. Then the aspect ratio (AR), the mean diameter, the standard deviation (SD) and the coefficient of variance (CV) were calculated for the characterization of nanoparticles assuming prolate shaped particles.

$$AR_i = d_{\text{major},i} / d_{\text{minor},i}$$

AR = mean value of  $AR_i$

$ESD = (d_{\text{major},i} * d_{\text{minor},i}^2)^{1/3}$  the equivalent spherical diameter

$\overline{ESD}$  mean diameter

$$SD = \sqrt{\frac{1}{N} \times \sum_{i=1}^N (ESD_i - \overline{ESD})^2}, \text{ with } N \text{ number of nanoparticles}$$

$$CV = SD / \overline{ESD}$$

### 4.3.2 UV-vis spectrum



Figure 4.9: Varian Cary 4000 UV-vis-NIR Spectrophotometer.<sup>45</sup>

This instrument provides the UV-vis-NIR spectrum from 175-900 nm with high resolution, and presents a wavelength accuracy of 0.1 nm.<sup>45</sup>

This spectrophotometer has three lamps: a deuterium lamp for UV spectrum (175-370 nm), a Tungsten lamp for VIS spectrum (370-750 nm) and part of NIR spectrum (750-900 nm), and a Mercury lamp that emits just a line spectrum.

A spectrophotometer UV-vis in its simplest form is composed by:

- 1) A light source
- 2) A monochromator
- 3) One or two cells
- 4) A detector
- 5) A readout

The instrument measures how much light is absorbed or reflected by a sample when it is irradiated by a radiation of known wavelength and a simple representation of how the spectrophotometer functions is in the fig. 4.10. This kind of interaction provides a qualitative analytic response (identification through the absorbed  $\lambda$ ), and a quantitative analytic response (through the Lambert Beer law for diluted solutions).

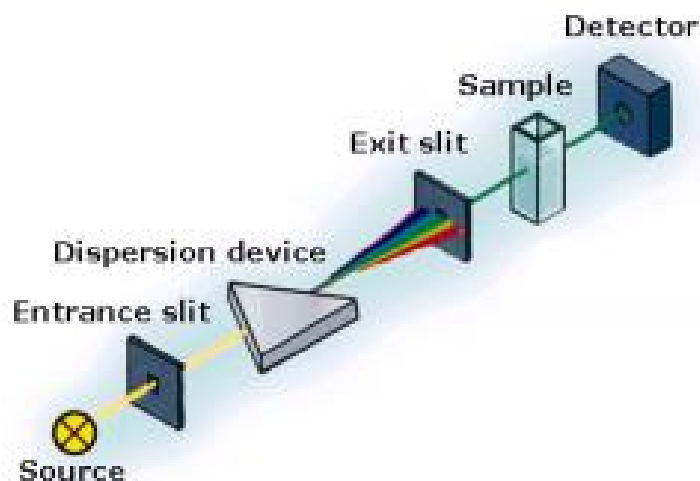


Figure 4.10: A simple representation of how a spectrophotometer functions.<sup>46</sup>

The sample is placed in the cell and absorbance vs wavelength is measured.

There are two main configurations for spectrophotometers: the single beam and the double beam. The single beam has a single path and it is necessary to switch manually the cuvette of reference (the blank) with the cuvette of the sample. In the double beam the light is split into the sample beam and reference beam.

In our experiments we used cuvette in PMMA for reference and samples, and the spectrophotometer in single beam configuration.

### Lambert Beer law

This law describes well the behavior in absorbance of diluted solutions, with concentration generally until 0.01M. Outside this limit, deviations are observed from the direct proportionality between absorbance and concentration.

$$A = \log \frac{I_0}{I} = \epsilon dC$$

A=absorbance (a.u.)

$\epsilon$ =molar extinction coefficient ( $M^{-1}cm^{-1}$ )

d= path length of the beam of light through the sample(cm)

C=concentration (M)

$T = \frac{I}{I_0} = 10^{-A}$ , is defined the transmittance that is measured in  $\%T = \frac{I}{I_0} \times 100$

$I_0$  is the intensity of light that enters the sample

$I$  is the intensity of light that goes out of the sample.

Usually the Lambert Beer law is used to determine the unknown concentration by measuring absorbance,  $C=A/\epsilon d$ .



## 5 Experimental section

### 5.1 Materials

To synthesize the colloidal gold nanoparticles, according to the Turkevich method, it is necessary to perform a hot injection of reducing/stabilizer agent into the water solution of the precursor salt  $\text{HAuCl}_4$  under stirring.

For the synthesis process the materials used in the lab are:

- a metallic gold foil 99.99% from Nuova Franco Swiss Italia.
- hydrogen chloride 37% in  $\text{H}_2\text{O}$ , 99,999% trace metals basis, by Sigma Aldrich.
- nitric acid 70%, purified by redistillation,  $\geq 99.999\%$ , trace metals basis, by Sigma Aldrich.
- sodium citrate tribasic dihydrate, ACS reagent,  $\geq 99.0\%$ , by Sigma Aldrich.
- citric acid, ACS reagent  $\geq 99.5\%$ , by Sigma Aldrich.
- aqua regia
- ultrapure water with  $18.2 \text{ M}\Omega\cdot\text{cm}$  at  $25 \text{ }^\circ\text{C}$  (MilliQ water)
- glass bottles to store the colloidal solutions

The  $\text{HAuCl}_4 \cdot 3\text{H}_2\text{O}$  stock solution was prepared by dissolving a gold foil into aqua regia solution as described in literature by S. Gross.<sup>47</sup>

In this experimental section, aqua regia and MilliQ water were used to clean the labware and stirring bars. Before each experiment MilliQ water was utilized to prevent the contaminations and overall as a solvent for all reactions.

### 5.2 Synthesis and method

The syntheses of the colloidal solutions were performed by changing the pH between the first and second reaction, using during the hot injection, a citrate water solution with the same concentration of citrate ions, but with different sodium ions concentration: a 100%  $\text{Na}_3\text{Cit}$ . solution is added in the first synthesis, and a 85% $\text{Na}_3\text{Cit}$  and 15% $\text{H}_3\text{Cit}$  solution is added in the second synthesis. In the third and fourth synthesis, with respect to the second, only the temperature at which is carried

out the rapid injection of the citrate solution is changed, into the hot  $\text{HAuCl}_4$  water solution.

|    |   |
|----|---|
| a) | 75 ml of 0.25 mM $\text{HAuCl}_4$ and 2.5 mM $\text{Na}_3\text{Cit}$ . water solution (MilliQ)<br><b>20.15mM of <math>\text{HAuCl}_4</math> stock solution</b><br><b>Hot injection at 70 °C of 500mM <math>\text{Na}_3\text{Cit}</math>. stock solution</b>   |
| b) | 75 ml of 0.25 mM $\text{HAuCl}_4$ and 2.5 mM $\text{H}_3\text{Cit}/\text{Na}_3\text{Cit}$ . (1:5) water solution (MilliQ)<br><b>20.15mM of <math>\text{HAuCl}_4</math> stock solution</b><br><b>Hot injection at 70 °C of 500mM <math>\text{H}_3\text{Cit}/\text{Na}_3\text{Cit}</math>. (1:5) stock solution</b>     |
| c) | 75 ml of 0.25 mM of $\text{HAuCl}_4$ + 2.5 mM of $\text{H}_3\text{Cit}/\text{Na}_3\text{Cit}$ . (1:5) water solution (MilliQ)<br><b>20.15mM of <math>\text{HAuCl}_4</math> stock solution</b><br><b>Hot injection at 60 °C of 500mM <math>\text{H}_3\text{Cit}/\text{Na}_3\text{Cit}</math>. (1:5) stock solution</b> |
| d) | 75 ml of 0.25 mM of $\text{HAuCl}_4$ + 2.5 mM of $\text{H}_3\text{Cit}/\text{Na}_3\text{Cit}$ . (1:5) water solution (MilliQ)<br><b>20.15mM of <math>\text{HAuCl}_4</math> stock solution</b><br><b>Hot injection at 50 °C of 500mM <math>\text{H}_3\text{Cit}/\text{Na}_3\text{Cit}</math>. (1:5) stock solution</b> |

Table 5.1: Synthesis conditions at the beginning of the reaction for each solution.

In the case a) when the  $\text{HAuCl}_4$  solution reaches the 70°C, a  $\text{Na}_3\text{Cit}$ . stock solution is injected, thus, the final solution becomes alkaline. In the case b) the temperature, and the concentrations of the precursor and the reducing agent, are the same, but the rapid injection at 70°C, is with a  $\text{H}_3\text{Cit}/\text{Na}_3\text{Cit}$  (1:5) stock solution, changing in this way only the pH.

In the last two cases only the temperature injection changes with respect to case b): the hot injection in the case c) occurs at 60°C and in the case d) at 50°C.

The steps of the syntheses are always the same: to the solution of water MilliQ is added a  $\text{HAuCl}_4$  stock solution, the obtained solution is heated at the desired temperature, at which it performs the injection of the reducing agent (that consists of  $\text{Na}_3\text{Cit}$  or a mixture of  $\text{H}_3\text{Cit}$  and  $\text{Na}_3\text{Cit}$ , according to the cases).

The final volume of the solution is about 75 ml. The reaction is stopped when the reduction potential and the pH reach the plateau that means all the precursor salt is reduced to  $\text{Au}^0$ .

### 5.3 Preparation phase

Preparation of 20.15 mM HAuCl<sub>4</sub> stock solution (provided by laboratory).

Preparation of 10ml of 500 mM Na<sub>3</sub>Cit stock solution:

$$0.500\text{mol/l} \times 294.1\text{g/mol} \times 10^{-2}\text{l} = 1.471\text{g of Na}_3\text{Cit. 2H}_2\text{O}$$

Dissolve 1.471g of Na<sub>3</sub>Cit. 2H<sub>2</sub>O in water (no CO<sub>2</sub>) and make up to 10ml the solution by adding water.

By the dilution equation  $C_1V_1=C_2V_2$ , we can calculate the volume of the stock solution ( $C_1, V_1$  are the concentration and the volume of the stock solution;  $C_2, V_2$  are the concentration and the volume of diluted solution)

$2.5\text{mM} \times 75\text{ml} / 500\text{mM} = \mathbf{0.375\text{ml}}$  volume of 500mM Na<sub>3</sub>Cit stock solution to inject, to have 75 ml of 2.5mM Na<sub>3</sub>Cit. and 0.25mM HAuCl<sub>4</sub> solution at the beginning of the synthesis.

$0.25\text{mM} \times 75\text{ml} / (75\text{ml} - 0.375\text{ml}) = 0.25\text{mM} \times 75\text{ml} / 74.625\text{ml} = 0.2512\text{mM}$  of HAuCl<sub>4</sub> in a volume of water (MilliQ) 74.625ml.

$74.625\text{ml} \times 0.2512\text{mM} = ? \times 20.15\text{mM} \rightarrow ? = 74.625\text{ml} \times 0.2512\text{mM} / 20.15\text{mM} = \mathbf{0.930\text{ml}}$ , volume of 20.15 HAuCl<sub>4</sub> stock solution to have 75 ml of 2.5mM Na<sub>3</sub>Cit. and 0.25mM HAuCl<sub>4</sub> solution at the beginning of the synthesis.

#### Protocol for (a) solution preparation

- (1)  $75\text{ml} - 0.930\text{ml} - 0.375\text{ml} = 75\text{ml} - 1.305\text{ml} = 73.695\text{ml}$  of water MilliQ
- (2) Add 0.930ml of 20.15 mM HAuCl<sub>4</sub> stock solution
- (3) Heat up to desired T
- (4) Rapidly inject 0.375ml of 500mM Na<sub>3</sub>Cit stock solution

#### Preparation of 10ml of 500mM H<sub>3</sub>Cit/Na<sub>3</sub>Cit (1:5) stock solution for the syntheses (b), (c), (d).

$$0.500\text{mol/l} \times 192.123\text{g/mol} \times 1/6 \times 10^{-2}\text{l} = 0.1601\text{g of H}_3\text{Cit.}$$

$$0.500\text{mol/l} \times 294.1\text{g/mol} \times 5/6 \times 10^{-2}\text{l} = 1.2254\text{g of Na}_3\text{Cit.}$$

Dissolve 0.1601g of H<sub>3</sub>Cit. and 1.2254g of Na<sub>3</sub>Ci 2H<sub>2</sub>O in water (no CO<sub>2</sub>) and make up to 10ml the solution by adding water.

#### Protocol for (b),(c),(d) solutions preparation

To have 75 ml of 2.5mM H<sub>3</sub>Cit/Na<sub>3</sub>Cit (1:5) and 0.25mM HAuCl<sub>4</sub> solution at the beginning of the synthesis:

- (1)  $75\text{ml} - 0.930\text{ml} - 0.375\text{ml} = 75\text{ml} - 1.305\text{ml} = 73.695\text{ml}$  of water MilliQ

- (2) Add 0.930ml of 20.15 mM HAuCl<sub>4</sub> stock solution
- (3) Heat up to desired T
- (4) Rapidly inject 0.375ml of 500mM H<sub>3</sub>Cit/Na<sub>3</sub>Cit (1:5) stock solution

## 5.4 Kinetic analysis

### 5.5 Reduction potential and pH measurements in situ

During the synthesis were carried out Eh (vs Ag/AgCl) and pH measurements, recording the values every 2 seconds.

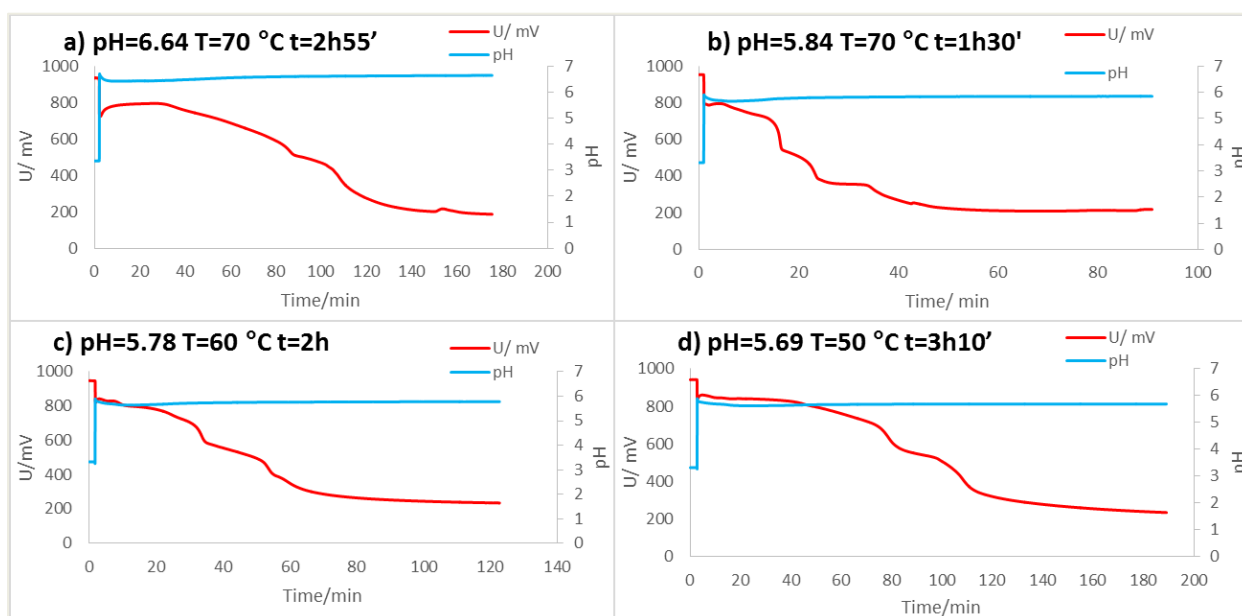


Figure 5.1: Measurements of Eh and pH of the solutions in situ

The reduction potential initially decreases rapidly, remains very positive around +0.8 V vs Ag/AgCl, during the nucleation, then Eh undergoes a longer reduction until to drop sudden at the end of the reaction at around 0.2 V, when the gold precursor is totally consumed. This occurs before the profile of UV-vis spectrum reaches its final form, and the synthesis is stopped. The change of Eh is correlated to the peptization of the particles: the formation of flocculated particles is followed by a peptization that is responsible of the monodisperse gold particles formation, and the drop of Eh that

occurs around 0.7 V, is precisely simultaneous to the moment in which the absorbance has a jump at 500-550 nm.

The values of pH in the reaction environments change from 3.3 to 6.69 (case a), to 5.84 (case b), to 5.78 (case c), to 5.69 (case d), passing through a peak and a depression in the first phase of the reaction, where the pH reaches a minimum value before increasing again toward the final value.

In the table 5.2 are reported some significative values of pH and the time.

| Reactions | pH                  | Time      |
|-----------|---------------------|-----------|
| a         | 3.3                 | 0         |
|           | 6.69 (max)          | 2.1 min   |
|           | 6.42 (min)          | 10 min    |
|           | 6.64 (=max)         | 2h55'     |
| b         | 3.3                 | 0         |
|           | 5.90 (max)          | 1 min     |
|           | 5.65 (min)          | 6.5 min   |
|           | 5.84 ( $\cong$ max) | 1h30'     |
| c         | 3.3                 | 0         |
|           | 5.89 (max)          | 1.86 min  |
|           | 5.64 (min)          | 11.46 min |
|           | 5.78 (<max)         | 2h        |
| d         | 3.3                 | 0         |
|           | 5.89 (max)          | 2.76 min  |
|           | 5.62 (min)          | 25.1 min  |
|           | 5.69 (<max)         | 3h10min   |

Table 5.2: Some significative values of pH during the reactions

The pH is one of the parameters that largely influences the nucleation and growth of AuNPs, as a consequence the change of pH causes the difference of the obtained data. According to Ji. et al., it is possible to distinguish two pathways of synthesis, based on the pH range: for low values of pH (3.7-6.5) the reaction is faster and the nanoparticles are more irregular in terms of size and shape; while for higher pH (6.5-7.7) the reaction of nucleation proceeds more slowly obtaining nanoparticles more regular. This because the pH influences the speciation of reagents, for lower pH the solution has a large amount of  $\text{AuCl}_4^-$  available for a faster nucleation; instead, for higher pH,  $\text{AuCl}_4^-$  shifts towards the idroxylated forms causing a slowing down of the

nucleation phase. The range of pH = 6.2-6.5 represents a switching point. In fact, for lower pH (3.7-6.5) the synthesis of AuNPs form through  $\text{AuCl}_3(\text{OH})^-$ , an intermediate more reactive, and it consists of three overlapping steps: fast nucleation, random attachment to polycrystalline nanowires and smoothing of nanowires via intraparticle ripening to dots. For higher pH (6.5-7.7) the gold AuNPs form through  $\text{AuCl}_2(\text{OH})_2^-$ ,  $\text{AuCl}(\text{OH})_3^-$ , intermediates less reactive, so the synthesis consists of a slow nucleation followed by slow growth.<sup>31,48</sup>

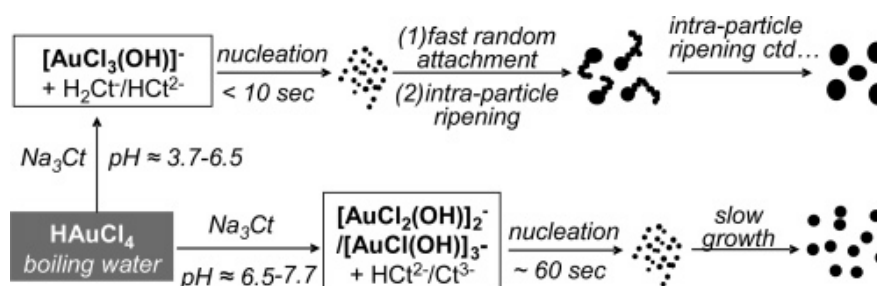


Figure 5.2: Scheme of two reaction pathway for the formation of gold nanoparticles by citrate reduction.<sup>48</sup>

In this experiment the variation of pH is due to the use of the citric acid  $\text{C}_6\text{H}_8\text{O}_7$  solution with the same molarity of  $\text{Na}_3\text{Cit}$  solution utilized in the synthesis, so as not to change the concentration of citrate ions taking part in the synthesis.

## 5.6 Temporal evolution of UV-vis spectrum

The synthesis phase was carried out recording the UV-vis spectra every 5 seconds. During the reaction it is observed the gradual increase of the SPR peak in the green-yellow light region (500-550 nm) that is correlated to the size and shape of nanoparticles. The curves shape changes, the band of the peak tends to become narrower and the peak undergoes before a red shift and finally a blue shift. In the range of 600-800 nm there is a flat band where the absorbance increases before to go to zero, and it is correlated to the transient gold nanowires formation, before the nanoparticles shrinkages reaching the final quasi spherical shape. Moreover the red light (above 600 nm) is absorbed mainly by that particles that grow largerly with respect to other, losing in this way the monodispersity of the colloidal solutions and the shape quasi-spherical of nanoparticles that exhibit irregular surfaces at the end of the synthesis.

During the reaction the solution changes color from yellow, before the injection, to colorless, that means the reduction is starting, to grey, grey-blue, blue that indicates the nanowires formation, and finally to ruby red, that means the quasi-spherical colloidal gold nanoparticle formation is complete.

The monitoring of evolution UV-vis spectrum during the synthesis of nanoparticles allows a qualitative and quantitative analysis with the possibility to extract the kinetic constants of reaction for nucleation and growth of AuNPs by using mathematic models, cited in literature.

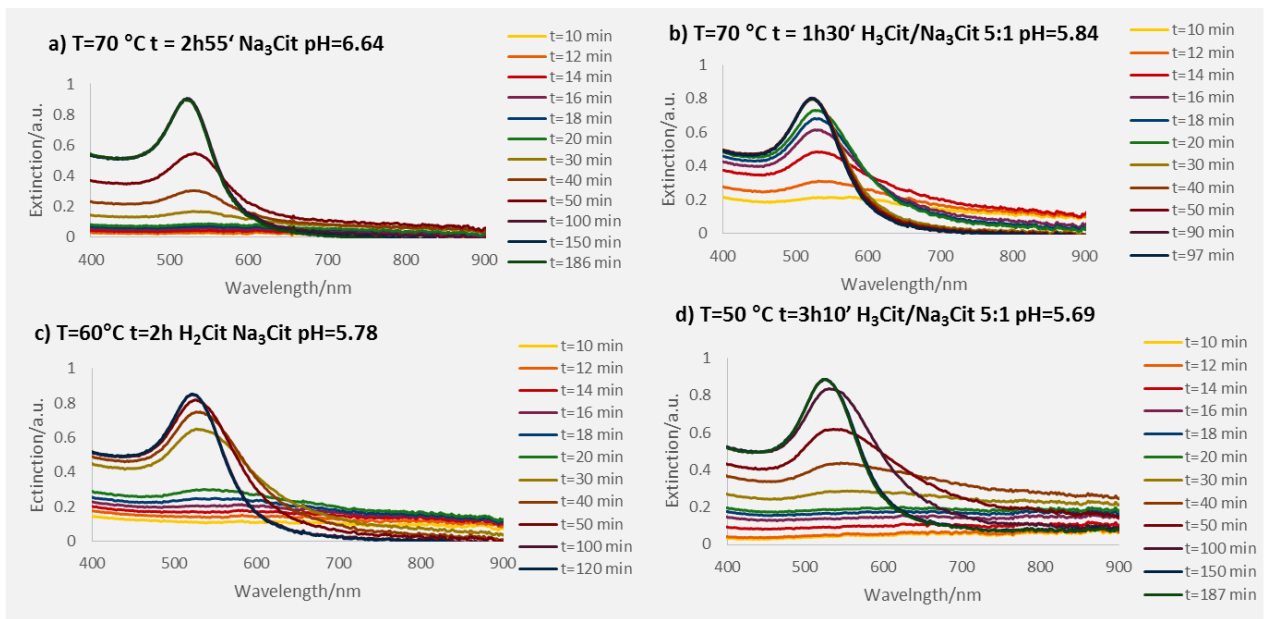


Figure 5.3: Temporal evolution of UV-vis spectrum during the syntheses of colloidal gold solutions

For a qualitative analysis of UV-vis spectrum, we will consider as an example, the case d).

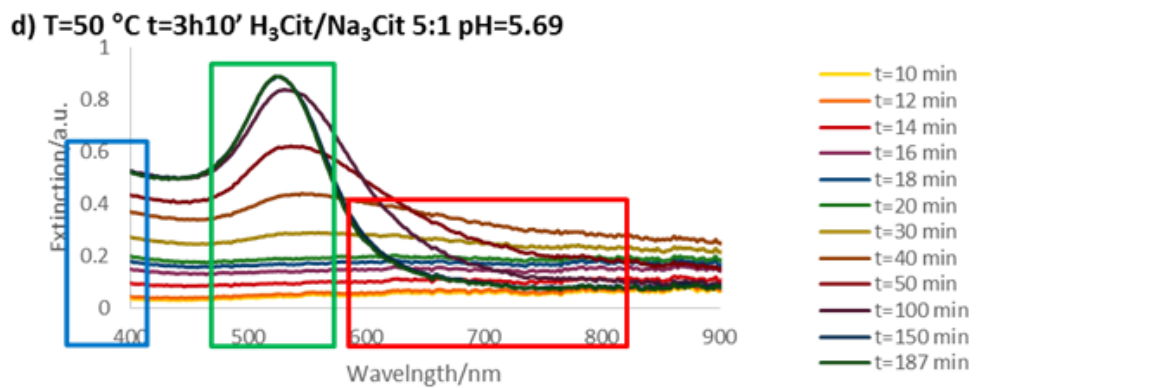


Figure 5.4: Illustration for a qualitative analysis of the synthesis of quasi-spherical gold nanoparticles through temporal evolution UV-vis spectrum.

The absorbance at 400nm has a linear relation with the concentration of  $Au^0$  in the solution.

The rise of absorbance between 600-800 nm is correlated to the formation of agglomerated nanoparticles that can aggregate in a reversible manner or not, synthesizing monodisperse (as the case a) or polydisperse (in case b), c), d)) systems.

In particular, the formation of monodisperse systems is favored when nucleation and growth take place separately, while an overlap of events leads to an increase in polydispersity. The red shift of SPR initially recorded, is correlated to the transient gold nanowires formation, whereas the blue shift of SPR that occurs later, is correlated to the particles that separate and shrink, forming charged quasi-spherical gold nanoparticle. The position of the peak SPR depends on the size and shape of NPs: a peak around 520 nm means that the particles are quasi-spherical and of 16-22 nm in diameter. The width of the peak indicates the degree of polydispersity of nanoparticles: a narrower peak means that the system is more monodisperse, while a broad peak is a sign of high polydispersity of the system.

For this reason a parameter frequently used to evaluate the polydispersity of NPs in solution, is the full width at half maximum calculated by UV-vis spectra and plotted as a function of time in fig.5.5.

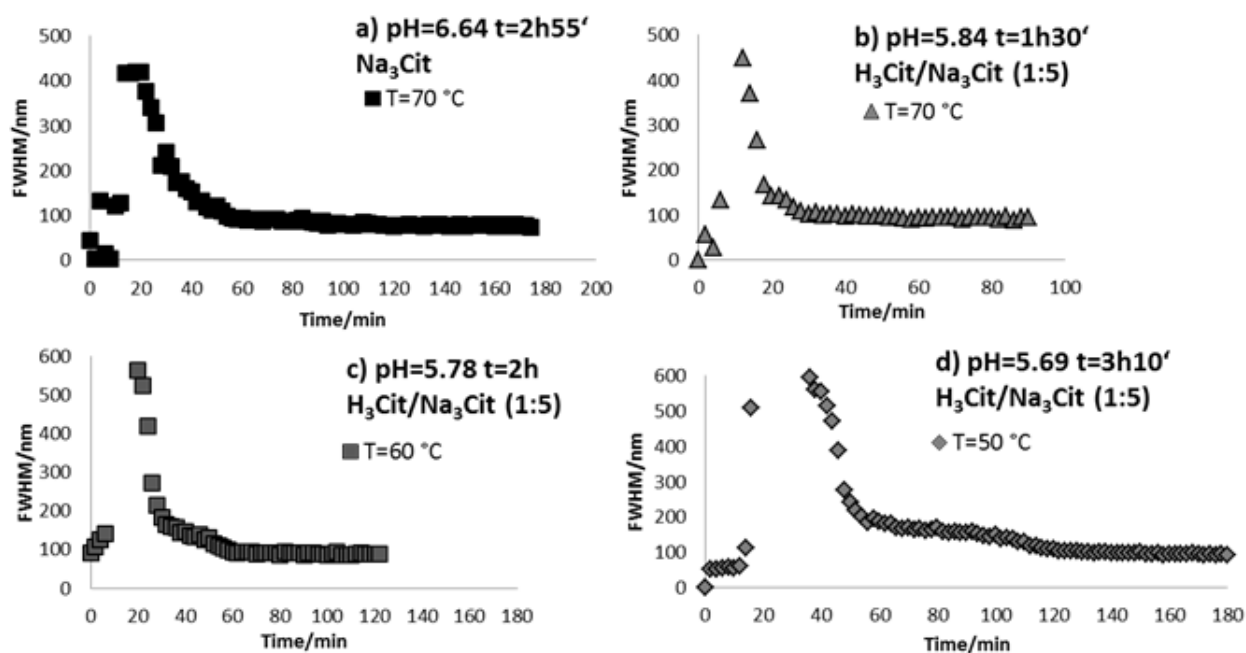


Figure 5.5: FWHM vs. time.  $FWHM = (\lambda_i - \lambda_{max}) * 2$ , where  $\lambda_i$  is the point of the  $Abs_{max}/2$  to the red of  $\lambda_{max}$ .<sup>49</sup>

The reduction in the FHMW parameter reflects the decrease in the degree of polydispersity during the formation of a monodisperse colloidal system. In this case, quasi-spherical gold particles have been synthesized. The curves show how the initially very polydisperse system, then evolves towards the final size of the nanoparticles with a homogeneous growth at high pH and heterogeneous growth at lower pH, obtaining a truly monodisperse system in the case of high pH (case (a)), and a system with greater polydispersity at lower pH (case (b)). The polydispersity increases largely for the syntheses c) and d) conducted with identical solutions to the case (b), but with lower injection temperature, to which competes slower reaction kinetics.

.

### 5.7 Morfological analysis (TEM)

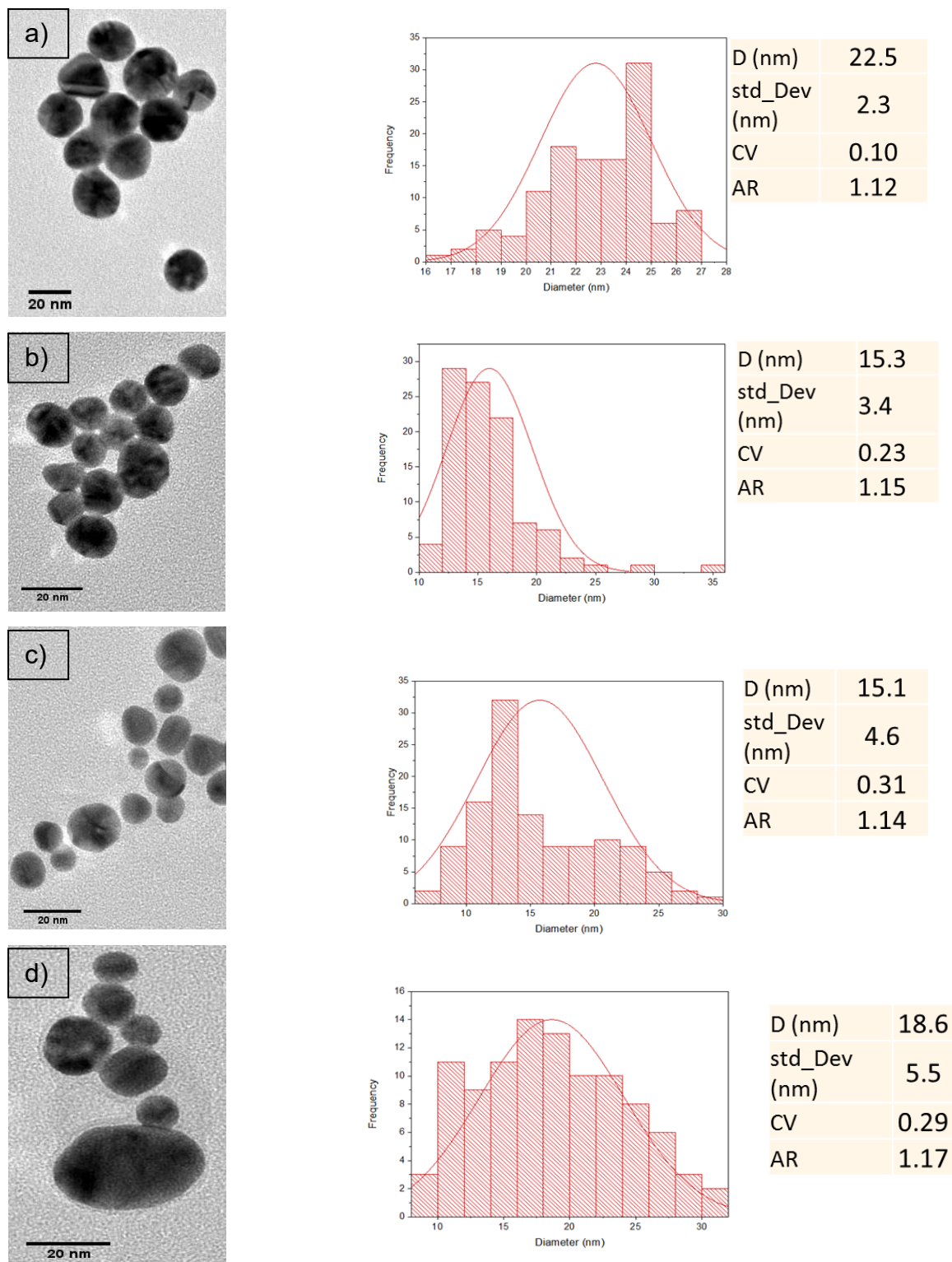


Figure 5.6: TEM micrographs ad histograms of gold nanoparticles.

The analysis are complete by transmission electron microscopy (TEM), that allows to see directly the nanoparticles and to study their morphology. For each prolate ellipsoid for at least 100 nanoparticles, has been calculated the aspect ratio (AR = ratio of major axis to transverse axis, that reflects the sphericity of NPs), the mean radius and the standard deviation with the coefficient of variance, that reflects the polydispersity of nanoparticles.

The synthesis conditions led to the formation of 16-22 nm diameter nanoparticles with a CV of 10% in case a) (monodisperse system with very regular particles), 23% in case b) (polydisperse system with less regular particles), and the polydispersity increases in the case c) and d) which have very irregular particles in shape and size.

| Samples* | UV-vis spectrum              |                              |           | TEM IMAGES + IMAGEJ (100 NPs)                    |                  |                         |                              |
|----------|------------------------------|------------------------------|-----------|--|------------------|-------------------------|------------------------------|
|          | Wavelength @ the SPR maximum | Absorbance @ the SPR maximum | FWHM (nm) | Aspect ratio $d_{\text{major}}/d_{\text{minor}}$ | Mean radius (nm) | Standard Deviation (nm) | Coefficient of variance CV % |
| a        | 522                          | 0.945503                     | 90        | 1.12   | 11.25            | 2.3                     | 10                           |
| b        | 522                          | 0.897079                     | 94        | 1.15   | 8                | 3.7                     | 23                           |
| c        | 520                          | 0.89276                      | 98        | 1.14   | 7.8              | 4.9                     | 31                           |
| d        | 524                          | 0.889058                     | 86        | 1.17   | 9.3              | 5.5                     | 29                           |

**Table 5.3: Characteristics of UV-vis spectrum, morphological parameters of AuNPs**

Comparing the characteristics of the UV-vis spectrum of the obtained colloidal systems, with the morphology of the NPs, we can do the following conclusions.

To an SPR peak around 522 nm, with absorption of about 0.9 and an FWHM around 90 nm, correspond quasi-spherical gold nanoparticles (AR around 1.12-1.15), which have an average radius between 8 and 11 nm, and are monodisperse at high pH, in this case 6.64 (CV 10%) and polydisperse at lower pH, for example 5.8 (CV 23%).

## 5.8 Kinetics and thermodynamics of nanoparticles nucleation and growth

The reaction kinetics are acquired by monitoring the change of absorbance at 400 nm by the temporal evolution of UV-vis spectrum, because at this wavelength the absorbance is linearly proportional to the  $\text{Au}^0$  concentration in the solution. The ratio between the absorbance at 400 nm and the maximum absorbance at 400 nm has

been plotted as a function of time and fitted by the reduction-crystallization model for gold nanoparticles, which come from by Finke Watzky model, that consists of two steps: slow continuous nucleation and autocatalytic growth:

$$A_t = A_{max} \left( 1 - \frac{k_1 + k_2}{k_2 + k_1 e^{(k_1 + k_2)t}} \right)$$

With  $k_1$  ( $s^{-1}$ ),  $k_2$  ( $s^{-1}$ ) nucleation and growth rate constants respectively.

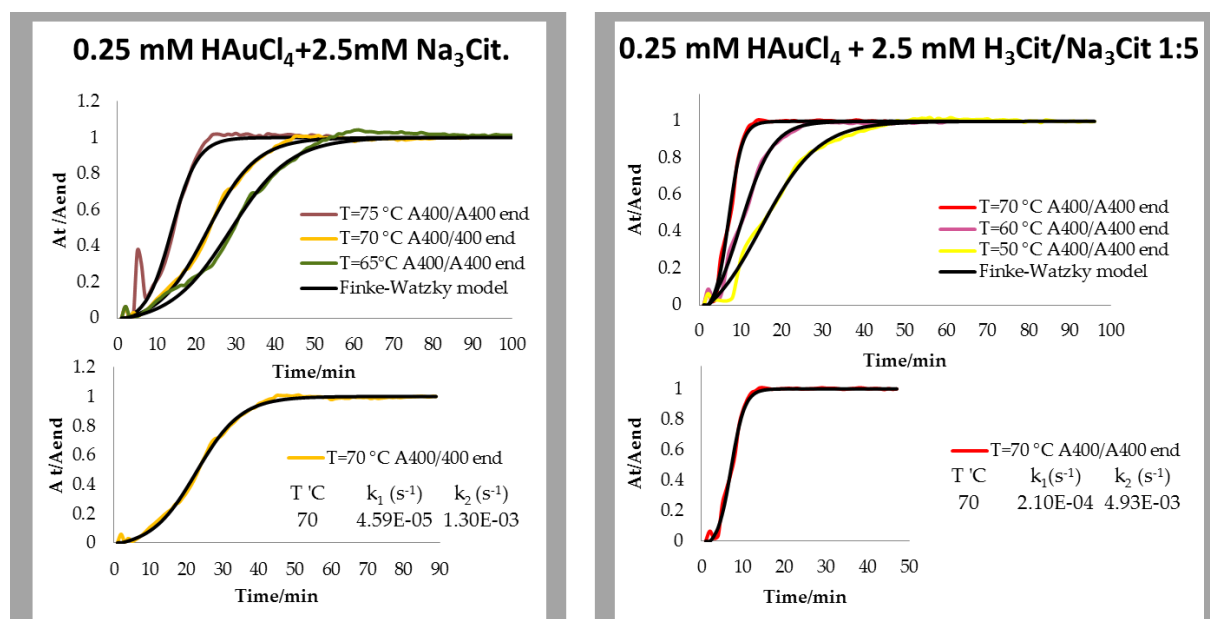


Figure 5.7: The kinetic curves of AuNPs formation

The kinetic curve exhibits a sigmoidal shape with three different stages:

- incubation period: reduction of Au(III) to Au (I) complex ions
- nucleation and growth: the absorbance rapidly rises for the reduction of Au(I) to Au(0)
- AuNPs formation

As an example, the rate constants have been reported for the syntheses carried out at a higher pH and at a lower pH with a injection temperature of 70°C, where the experimental data describe a profile of the curves that is well fitted by the mathematical model (black curve).

Through the Arrhenius equation, it is possible to calculate the activation energy for the nucleation and growth, by considering the kinetic constants obtained by the Finke-Watzky model.

By Arrhenius law:

$$k_1 = K_{0,1} e^{\left[-\frac{E_{a,1}}{RT}\right]} \text{ for particles nucleation}$$

$$k_2 = K_{0,2} e^{\left[-\frac{E_{a,2}}{RT}\right]} \text{ for particles growth}$$

Where  $K_{0,i}$  is the pre-exponential factor, and  $E_{a,i}$  the activation energy,  $T$  is the temperature in Kelvin, and  $R$  is the universal gas constant (8.31 J/(molK)). Rearranging, the equations become:

$$\ln k_1 = \ln k_{o,1} - \frac{E_{a,1}}{RT}$$

$$\ln k_2 = \ln k_{o,2} - \frac{E_{a,2}}{RT}$$

Plotting  $\ln k_i$  vs  $1/T$  (in Kelvin), the linear regression of the experimental data shows a slope that is  $-\frac{E_{a,i}}{R}$ , so multiplying the value of the slope of the line for  $R$ , we can obtain the energy activation for nucleation and growth.

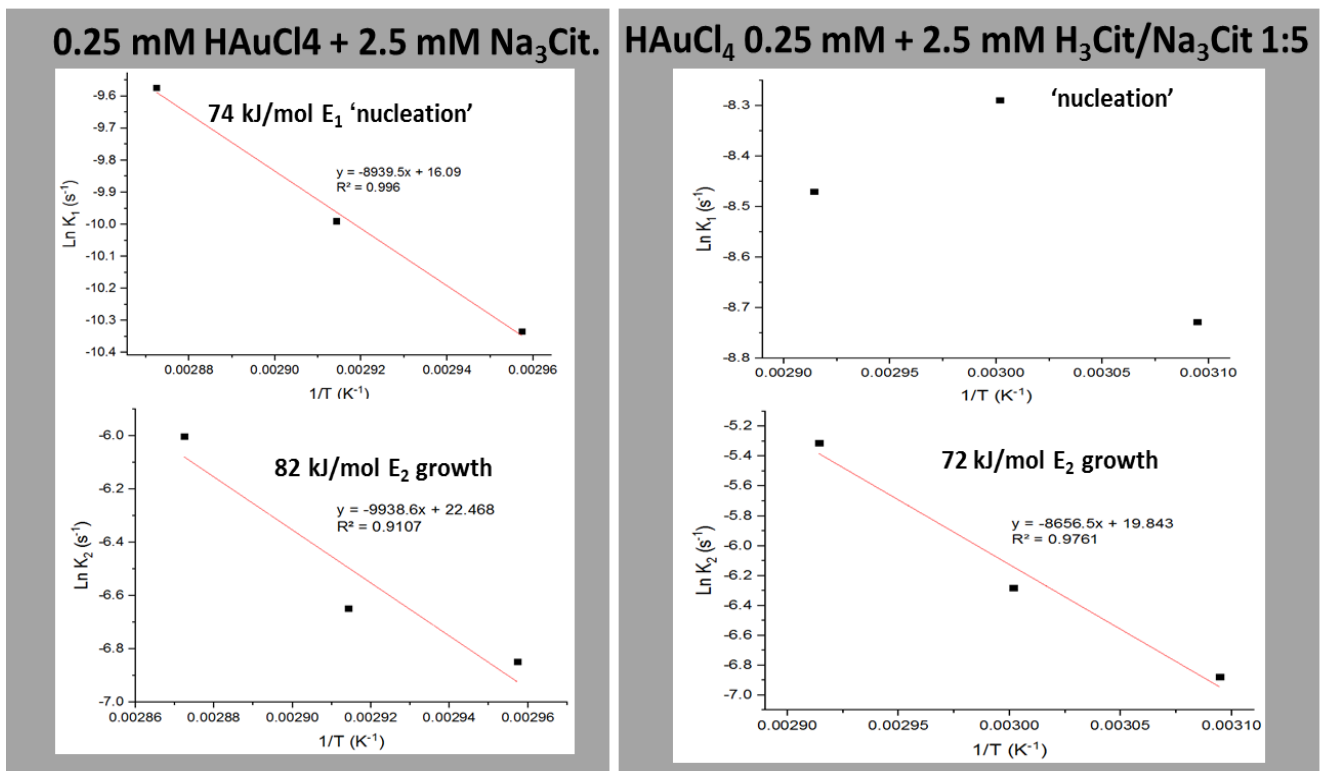


Figure 5.8: Plots of  $\ln k$  vs  $1/T$  to determine the activation energies in conditions of higher pH (on left) and of lower pH (on right).

In the case of synthesis via injection of 100% Na<sub>3</sub>Cit solution, it is possible to fit, with the linear function of Arrhenius in logarithm scale, the data in the plot of the logarithm of kinetic rates, as function of the inverse of temperature in Kelvin.

The slope of the line is proportional to the energy of the process of nucleation and growth, when are used  $K_1$  and  $K_2$  respectively, calculated in excel by using F-W model.

### 5.9 Conclusions

This F-W model reveals inconsistent for the description of syntheses carried out with the injection of  $H_3Cit/Na_3Cit$  (1:5) solution, where the resulting pH favors the formation of  $AuCl_4^-$ , that is more reactive of the hydroxylated complex ions of Au(III) ( $[AuCl_{4-x}(OH)_x]^-$ ).

A greater quantity of  $AuCl_4^-$  ions, causes the aggregation of NPs, because promotes the NPs mobility, and lowers their colloidal stability, thus the synthesis proceeds via nucleation, random attachment and intraparticle ripening

Within the first minutes after the injection, only a small fraction of  $AuCl_4^-$  ions, is consumed by citrate for the formation of seeds, the remaining part is adsorbed on the NPs and this occurs at the beginning of the nucleation; while the adsorption of citrate occurs at the end. The  $AuCl_4^-$  ions don't promote the colloidal stability of NPs, because the electrostatic repulsion is not sufficient, and this causes the agglomeration of newly formed NPs. The electrostatic repulsion, responsible of the colloidal stability and the peptization of agglomerate NPs, occurs when these are coated mainly by citrate. Therefore, in the syntheses in which the formation of  $AuCl_4^-$  ions is more favored with respect to  $[AuCl_{4-x}(OH)_x]^-$  ions, the sphericity and the monodispersity of the final NPs, are compromised. The kinetics of processes of nucleation and growth is accelerated, and the two processes enter in competition leading to the formation of a non monodispersed system.

Instead, a greater quantity of Au(III) in idroxylated form with respect to  $AuCl_4^-$ , leads to the precipitation of Au(III) complex ions (less reactive) exclusively on the surface defects of NPs that are flocculating. Probably the monodispersity of colloidal gold is due to the difference of reactivity of species of Au (III) that can promote the separation of the processes of nucleation and growth.

Once the first NPs have formed, via a homogeneous nucleation through the reduction of  $AuCl_4^-$  in solution, according to the reactivity of auric species in excess

presented in the solution, the active sites of AuNPs surfaces can act as center for a fast nucleation, intraparticle growth and fast growth or for a slower nucleation and fast growth.

This model of NPs nucleation and growth is in contrast with the CNT, because it depends on the colloidal stability, and it explains the enormous color change of the solution during the synthesis.

An important aspect of colloidal gold stabilized by citrate, is that the citrate ions are weakly bound to the AuNPs surface, making very easy the functionalization of the surfaces with other ligands



---

## References

1. Schaming, D. & Remita, H. Nanotechnology: from the ancient time to nowadays. *Found. Chem.* **17**, 187–205 (2015).
2. Feynman, R. P. *Caltech Engineering and Science.* **23:5** 22–36 (1960).
3. IBM.: <https://www-03.ibm.com/press/us/en/photo/28500.wss>.
4. sigma-aldrich. <https://www.sigmaaldrich.com/technical-documents/articles/materials-science/nanomaterials/quantum-dots.html>.
5. Sattler, K. *The energy gap of clusters, nanoparticles, and quantum dots. Handbook of Thin Films* **5**, (2007).
6. Wang, X. *et al. Encyclopedia of Nanoscience and Nanotechnology.* **1**, (2007).
7. Gupta, S. K., Talati, M. & Jha, P. K. Shape and Size Dependent Melting Point Temperature of Nanoparticles. *Mater. Sci. Forum* **570**, 132–137 (2009).
8. M., P., Caro, C., Klippstein, R., P., A. & Pozo, D. Silver Nanoparticles: Sensing and Imaging Applications. *Silver Nanoparticles* (2012). doi:10.5772/8513
9. Khan, A. K., Rashid, R., Murtaza, G. & Zahra, A. Gold nanoparticles: Synthesis and applications in drug delivery. *Tropical Journal of Pharmaceutical Research* (2014). doi:10.4314/tjpr.v13i7.23
10. sigma-aldrich. <https://www.sigmaaldrich.com/technical-documents/articles/materials-science/nanomaterials/gold-nanoparticles.html>.
11. Rad, A. G., Abbasi, H. & Afzali, M. H. Gold nanoparticles: Synthesising, characterizing and reviewing novel application in recent years. *Phys. Procedia* **22**, 203–208 (2011).
12. Zhong, C. *et al. Catalysts for Fuel Cell Reactions.* 289–307 (2000).
13. Hong, X., Tan, C., Chen, J., Xu, Z. & Zhang, H. Synthesis, properties and applications of one- and two-dimensional gold nanostructures. *Nano Res.* **8**, 40–55 (2014).
14. Yah, C. S. The toxicity of gold nanoparticles in relation to their physiochemical properties. *Biomed. Res.* **24**, 400–413 (2013).
15. Shah, M. Gold nanoparticles: various methods of synthesis and antibacterial applications. *Front. Biosci.* **19**, 1320 (2014).
16. Waters, C. A., Mills, A. J., Johnson, K. A. & Schiffrin, D. J. Purification of dodecanethiol derivatised gold nanoparticles. *Chem. Commun.* **3**, 540–541 (2003).
17. Voliani, V. Update on Gold Nanoparticles. **44**, 156 (2013).
18. Xia, H., Bai, S., Hartmann, J. & Wang, D. Synthesis of monodisperse quasi-spherical gold nanoparticles in water via silver(I)-assisted citrate reduction. *Langmuir* **26**, 3585–3589 (2010).
19. Xia, H., Xiahou, Y., Zhang, P., Ding, W. & Wang, D. Revitalizing the Frens Method to Synthesize Uniform, Quasi-Spherical Gold Nanoparticles with Deliberately Regulated Sizes from 2 to 330 nm. *Langmuir* **32**, 5870–5880 (2016).
20. Wuithschick, M. *et al. Turkevich in New Robes: Key Questions Answered for the Most Common Gold Nanoparticle Synthesis.* *ACS Nano* **9**, 7052–7071 (2015).

## REFERENCES

---

21. Takiyama, K. Formation and Aging of Precipitates. VIII. Formation of Monodisperse Particles (1) Gold Sol Particles by Sodium Citrate Method. *Bull. Chem. Soc. Jpn.* **31**, 944–950 (2006).
22. Chow, M. K.; Zukoski, C. F. Gold Sol Formation Mechanisms: Role of Colloidal Stability. *J. Colloid Interface Sci.* 1994, 165, 97–109.
23. Polte, J. Fundamental growth principles of colloidal metal nanoparticles - a new perspective. *CrystEngComm* **17**, 6809–6830 (2015).
24. Patungwasa, W. & Hodak, J. H. pH tunable morphology of the gold nanoparticles produced by citrate reduction. *Mater. Chem. Phys.* **108**, 45–54 (2008).
25. Kettemann, F. *et al.* Missing Piece of the Mechanism of the Turkevich Method: The Critical Role of Citrate Protonation. *Chem. Mater.* **28**, 4072–4081 (2016).
26. Smirnov, E. *Assemblies of gold nanoparticles at liquid-liquid interfaces: from liquid optics to electrocatalysis.* **7477**, (2017).
27. Rodríguez-González, B., Mulvaney, P. & Liz-Marzán, L. M. An electrochemical model for gold colloid formation via citrate reduction. *Zeitschrift fur Phys. Chemie* **221**, 415–426 (2007).
28. Rodríguez-Fernández, J., Pérez-Juste, J., Mulvaney, P. & Liz-Marzán, L. M. Spatially-directed oxidation of gold nanoparticles by Au(III)-CTAB complexes. *J. Phys. Chem. B* **109**, 14257–14261 (2005).
29. Mullin, J. W. *Crystallization, 4th Edition, Butterworth-Heinemann, Oxford.* (2011).
30. Cao, G. *Nanostructures and nanomaterials: Synthesis, Properties and Applications, Imperial College Press, London.* (2004). doi:10.1142/9781860945960
31. Thanh, N. T. K., Maclean, N. & Mahiddine, S. Mechanisms of Nucleation and Growth of Nanoparticles in Solution. *Chem. Rev.* **114**, 7610–7630 (2014).
32. Kwon, S. G. & Hyeon, T. Formation mechanisms of uniform nanocrystals via hot-injection and heat-up methods. *Small* **7**, 2685–2702 (2011).
33. Sugimoto, T. *Monodispersed Particles; Elsevier: Amsterdam.* (2001).
34. Dunne, P. W., Munn, A. S., Starkey, C. L., Huddle, T. A. & Lester, E. H. Continuous-flow hydrothermal synthesis for the production of inorganic nanomaterials. *Philos. Trans. R. Soc. A Math. Phys. Eng. Sci.* **373**, (2015).
35. Xia, Y., Xiong, Y., Lim, B. & Skrabalak, S. E. Shape-Controlled Synthesis of Metal Nanocrystals: Simple Chemistry Meets Complex Physics? *Angew Chem Int Ed* **48**, 60–103 (2009).
36. Paclawski, K., Streszewski, B., Jaworski, W., Luty-Błocho, M. & Fitzner, K. Gold nanoparticles formation via gold(III) chloride complex ions reduction with glucose in the batch and in the flow microreactor systems. *Colloids Surfaces A Physicochem. Eng. Asp.* **413**, 208–215 (2012).
37. Watzky, M. A. & Finke, R. G. Transition metal nanocluster formation kinetic and mechanistic studies. A new mechanism when hydrogen is the reductant: Slow, continuous nucleation and fast autocatalytic surface growth. *J. Am. Chem. Soc.* **119**, 10382–10400 (1997).
38. Zhou, Y. *et al.* Quantitative nucleation and growth kinetics of gold nanoparticles via model-assisted dynamic spectroscopic approach. *J. Colloid Interface Sci.* **407**, 8–16 (2013).
39. Watzky, M. A. & Finke, R. G. Gold Nanoparticle Formation Kinetics and Mechanism: A Critical

- 
- Analysis of the 'redox Crystallization' Mechanism. *ACS Omega* **3**, 1555–1563 (2018).
40. Metrohm Titrand 907. <https://www.metrohm.com/en-sg/documents/89078003>
  41. Ocean optics. <https://oceanoptics.com/product/dh-mini/>
  42. Ocean optics. <https://oceanoptics.com/product/flame-spectrometer>
  43. Ocean optics. <https://oceanoptics.com/product/t300-series-transm>
  44. ThetaMetrisis. <https://www.thetametrisis.com/technology/optical-m>
  45. Varian Cary 4000. <http://www.medwv.com/med/spectrophotometer/varian>
  46. Kerszulis, J. A. Cary UV/Vis/NIR 5000. *Mater. Sci.* **33** (2012).
  47. Gross, S. *Colloidal dispersion of gold nanoparticles. Materials Syntheses: A Practical Guide* (Springer Vienna, 2008). doi:10.1007/978-3-211-75125-1\_21
  48. Ji, X. *et al.* Size control of gold nanocrystals in citrate reduction: the third role of citrate. Supporting Information. *J. Am. Chem. Soc.* **5–6** (2007).
  49. Brown, K. R., Walter, D. G. & Natan, M. J. Seeding of colloidal Au nanoparticle solutions. 2. Improved control of particle size and shape. *Chem. Mater.* **12**, 306–313 (2000).